

# GlucoSynth: Generating Differentially-Private Synthetic Glucose Traces

Josephine Lamp<sup>1,2</sup> Mark Derdzinski<sup>2</sup> Christopher Hannemann<sup>2</sup> Joost van der Linden<sup>2</sup> Lu Feng<sup>1</sup>  
Tianhao Wang<sup>1</sup> David Evans<sup>1</sup>

## Abstract

In this paper we focus on the problem of generating *high-quality, private* synthetic glucose traces, a task generalizable to many other time series sources. Existing methods for time series data synthesis, such as those using Generative Adversarial Networks (GANs), are not able to capture the innate characteristics of glucose data and, in terms of privacy, either do not include any formal privacy guarantees or, in order to uphold a strong formal privacy guarantee, severely degrade the utility of the synthetic data. Therefore, in this paper we present GlucoSynth, a novel privacy-preserving GAN framework to generate synthetic glucose traces. The core intuition in our approach is to conserve relationships amongst motifs (glucose events) within the traces, in addition to typical temporal dynamics. Moreover, we integrate differential privacy into the framework to provide strong formal privacy guarantees. Finally, we provide a comprehensive evaluation on the real-world utility of the data using 1.2 million glucose traces.

## 1. Introduction

The sharing of medical time series data can facilitate therapy development. As a motivating example, sharing glucose traces can contribute to the understanding of diabetes disease mechanisms and the development of artificial insulin delivery systems that improve people with diabetes’ quality of life. Unsurprisingly, there are serious, well-documented legal and privacy concerns (e.g., HIPAA, GDPR) with the sharing of such granular, longitudinal time series data (Britton & Britton-Colonnese, 2017). One solution is to generate a set of synthetic time series from the original traces. In this way, the synthetic data may be shared publicly in place of the real ones, significantly reducing privacy/legal concerns.

This paper focuses on the problem of generating *high-quality, private* synthetic glucose traces, a task which generalizes to other time series sources and application domains, including activity sequences, inpatient events, hormone traces and cyber-physical systems. Specifically, we focus on long (>200 timesteps), bounded, univariate glucose traces. We assume that available data does not have any labels or extra information including features or metadata, which is quite common, especially in diabetes. Continuous Glucose Monitors (CGMs) easily and automatically send glucose measurements taken subcutaneously at fixed intervals (e.g., every 5 minutes) to data storage facilities. However, tracking other sources of diabetes-related data is challenging (Young-Hyman et al., 2016). We characterize “high-quality” as follows, based on three criteria: synthetic traces should conserve characteristics of the real data, e.g., glucose dynamics and control-related metrics (**fidelity**); contain representation of diverse *types* of traces, without the introduction of anomalous patterns not contained in the original data (**breadth & data artifacts**); and be usable in place of the original data for real-world use cases (**utility**).

Generative Adversarial Networks (GANs) (Goodfellow et al., 2020) have shown promise in the generation of time series data. However, previous methods for time series synthesis, e.g., (Yoon et al., 2019; Li et al., 2022), suffer from one or more of the following issues when applied to glucose traces: 1) surprisingly, they do not generate realistic synthetic glucose traces – in particular, they produce human physiologically impossible phenomenon in the traces; 2) they require additional information (extra features, metadata or labels) to guide the model learning which are not available for our traces; 3) they do not include any privacy guarantees, or, in order to uphold a strong formal privacy guarantee, severely degrade the utility of the synthetic data.

Generating high-quality synthetic glucose traces is a difficult task due to the innate characteristics of glucose data. Glucose traces can be best understood as sequences of events, which we call *motifs*, shown in Figure 1, and they are more event-driven than many other types of time series. As such, a current glucose value may be more influenced by an event that occurred in the far past compared to values from immediate previous timesteps. For example, a large meal eaten earlier in the day (30-60+ minutes ago) may influence a

<sup>1</sup>Department of Computer Science, University of Virginia, VA, USA <sup>2</sup>Dexcom, USA. Correspondence to: Josephine Lamp <jl4rj@virginia.edu>.

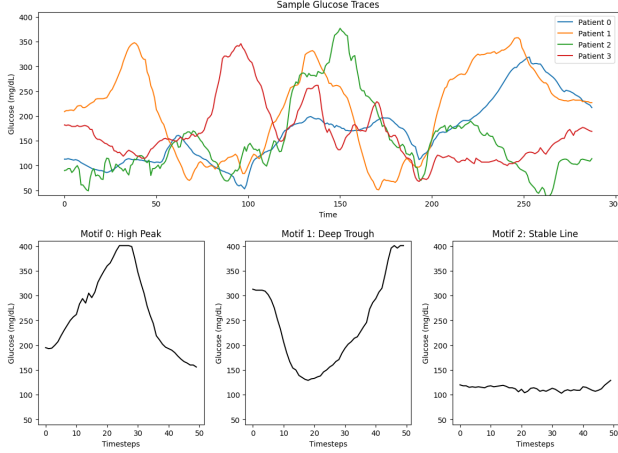


Figure 1. Sample Glucose Traces and Example Glucose Motifs.

patient’s glucose more than the glucose values from the past 15 minutes. As a result, although there is some degree of temporal dependence within the traces, *only* conserving the immediate temporal relationships amongst values at previous timesteps may not best capture the dynamics of this type of data. In particular, we find that the main reason previous methods fail is because they may not sufficiently learn event-related characteristics of glucose traces.

In this paper, we present **Glucosynth**, a privacy-preserving GAN framework to generate synthetic glucose traces. The core intuition behind our approach is to conserve relationships amongst motifs (events) within the traces, in addition to the typical temporal dynamics contained within time series. Moreover, we provide an integrated privacy-preserving methodology as part of the framework that employs the use of *differential privacy* (Dwork, 2008), which provides an intuitive bound on how much information may be disclosed about any individual in the dataset.

Specifically, we present the following contributions: (1) We formalize the concept of motifs and define a notion of *motif causality*, inspired from Granger causality (Granger, 1969), which characterizes relationships amongst sequences of motifs within time series traces. We define a local motif loss to first train a motif causality block that learns the motif causal relationships amongst the sequences of motifs in the real traces. The block outputs a motif causality matrix, that quantifies the causal value of seeing one particular motif after some other motif. Unrealistic motif sequences (such as a peak to an immediate drop in glucose values) will have causal relationships close to 0 in the causality matrix. (2) We build a novel GAN framework that is trained to optimize motif causality within the traces in addition to temporal dynamics and distributional characteristics of the data. Specifically, the generator computes a motif causal matrix on each batch of synthetic data it generates, and compares it with the real causality matrix. As such, as the generator learns to generate synthetic data that yields a real-

istic causal matrix (thereby identifying appropriate causal relationships from the motifs), it implicitly learns not to generate unrealistic motif sequences. This framework produces high-quality, realistic synthetic glucose traces. (3) We provide an integrated differential privacy framework allowing the Glucosynth model to be trained with privacy guarantees. (4) We present a comprehensive evaluation using 1.2 million glucose traces from individuals with diabetes collected across 2022, showcasing the suitability of our model to outperform all previous models and generate high-quality synthetic glucose traces with strong privacy guarantees.

## 2. Related Work

We focus the scope of our comparison on current state-of-the-art methods for synthetic time series which all build upon Generative Adversarial Networks (GANs) (Goodfellow et al., 2020) and transformation-based approaches (Dinh et al., 2016). An extended related work is in Appendix A.

**Time Series.** Brophy et al. (2021) provides a survey of GANs for time series synthesis. TimeGAN (Yoon et al., 2019) is a popular benchmark that jointly learns an embedding space using supervised and adversarial objectives in order to capture the temporal dynamics amongst traces. Esteban et al. (2017) develops two time series GAN models (RGAN/RCGAN) with RNN architectures, conditioned on auxiliary information provided at each timestep during training. TTS-GAN (Li et al., 2022), trains a GAN model that uses a transformer encoding architecture in order to best preserve temporal dynamics. Transformation-based approaches such as real-valued non-volume preserving transformations (NVP) (Dinh et al., 2016) and Fourier Flows (FF) (Alaa et al., 2021), have also had success for time series data. These methods model the underlying distribution of the real data to transform the input traces into a synthetic data set. Methods that only focus on learning the temporal or distributional dynamics in time series are not sufficient for generating *realistic* synthetic glucose traces due to the lack of temporal dependence within sequences of glucose motifs.

**Differentially-Private GANs.** To protect sensitive data, several GAN architectures (DP GANs) have been designed to incorporate privacy-preserving noise needed to satisfy differential privacy guarantees (Xie et al., 2018). Frigerio et al. (2019) extends a simple DP GAN architecture (denoted dpGAN) to time-series data and RDP-CGAN (Torfi et al., 2022) develops a convolutional GAN architecture that uses Rényi differential privacy specifically for medical data. These methods find large gaps in performance between the nonprivate and private models and, in some cases, providing strong theoretical DP guarantees results in destroying the fidelity of the synthetic data, beyond anything feasible for use in real-world scenarios. Our DP framework uses two different methods to integrate privacy, resulting in a better

utility-privacy trade off than previous methods.

### 3. Preliminaries

#### 3.1. Motifs

We denote a set of  $n$  time series traces  $X = [x_1, \dots, x_n]$ . Glucose (and many other) traces can be best understood as sequences of events or *motifs*. Such motifs characterize phenomenon in the traces, such as peaks or troughs. We define a *motif*,  $\mu$ , as a short, ordered sequence of values ( $v$ ) of specified length  $\tau$ ,

$$\mu = [v_i, v_{i+1}, \dots, v_{i+\tau}]$$

and  $\sigma$  is a tolerance value to allow approximate matching (within  $\sigma$  for each value). Throughout the entire paper we assume a tolerance of  $\sigma = 2$  mg/dL, chosen to allow for reasonable variations in glucose. Real example glucose motifs are shown in the bottom row of Figure 1.

A time series may be represented as a sequence of motifs:  $x_i = [\mu_{i_1}, \mu_{i_2}, \dots]$  where each  $i_j$  gives the index of the motif in the set that matches  $x_{i_j}, \dots, x_{i_{j+1} \cdot \tau - 1}$ . Given the motif length  $\tau$ , the motif set is the union of all size- $\tau$  chunks in the traces. This definition is chosen for a more straightforward implementation. However, motifs can be generated in other ways, such as through the use of a rolling window or using signal processing techniques. Motifs are summarized from the data such that there is always a match between a glucose motif and a motif from the set; if matched to multiple, it is matched to the one with the least changes.

#### 3.2. A Study in Glucose Dynamics - Why Models Fail

We first present a study of the characteristics of glucose data in order to motivate the development of our framework. Although there are general patterns in sequences of glucose motifs (e.g., motif patterns corresponding to patients that eat 2x vs. 3x a day), individual glucose motifs are not time-dependent. This is illustrated in Figure 2. Each radial graph displays the temporal distribution of a motif; there are 24 radial bars from 00:00 to 23:00 for each hour of the day, and the bar value is the percentage of total motif occurrences at that hour across the entire dataset (e.g., value of 10 indicates 10% of the time that motif occurs at that hour). The first two motifs are real glucose motifs sampled from our dataset’s motif set; these motifs show up *across* hours of the day. Compare this to the bottom two time-dependent motifs pulled from a real cardiology dataset (Binanay et al., 2005). These motifs have shifts in their distribution; they show up frequently at *specific* hours of the day.

The lack of temporal dependence in glucose motifs is likely due to the diverse patient behaviors within a patient population. Glucose in particular is highly variable and influenced by many factors including eating habits, exercise, stress

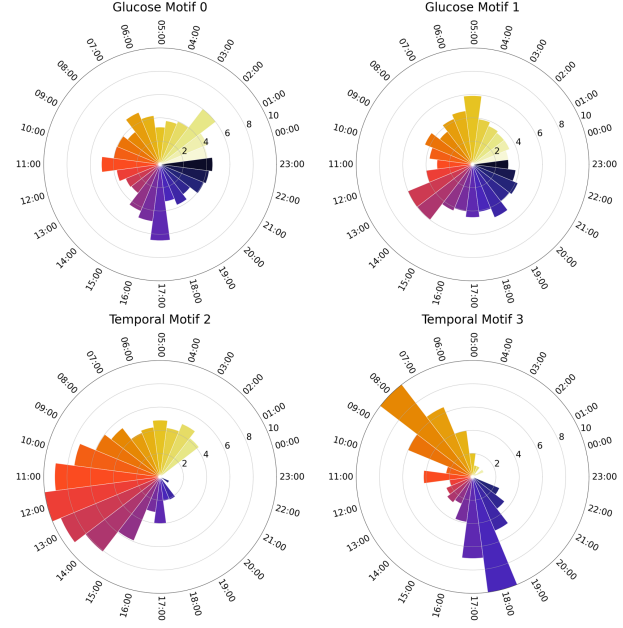


Figure 2. Temporal Distributions of Sample Motifs. Each radial graph displays the percentage of motif occurrences by each hour for each motif. The top row shows two real glucose motifs sampled from our glucose traces; they are not temporally dependent and show up across the day. The bottom row shows example temporally dependent motifs from a cardiology dataset (Binanay et al., 2005).

levels, sleep patterns, etc. Moreover, due to the innate variability within human physiology, occurrences of these motifs can differ even for the *same* patient across weeks or months. These findings indicate that only conserving the temporal relationships within glucose traces (as many previous methods do,) may not be sufficient to properly learn glucose dynamics and output realistic synthetic traces.

#### 3.3. Granger Causality

Granger causality is a common framework used to quantify relationships amongst time series without limiting the degree to which temporal relationships may be understood as done in other time series models (e.g., pure autoregressive ones.) In this framework, an entire system (set of traces) is studied *together*, allowing for a broader characterization of their relationships, which may be advantageous, especially for long time series. We define  $x_t \in \mathbb{R}^n$  as an  $n$ -dimensional vector of time series traces observed across  $n$  traces and  $T$  timesteps. To study Granger Causality, a vector autoregressive model (VAR) (Lütkepohl, 2005) may be used: a set of traces at time  $t$  is represented as a linear combination of the previous  $K$  lags in the series

$$x_t = \sum_{k=1}^K A^{(k)} x_{t-k} + e_t$$

where each  $A^{(k)}$  is a  $n \times n$  dimensional matrix that describes how lag  $k$  affects the future timepoints in the series’ and  $e_t$

is a zero mean noise. Given this framework, we state that time series  $q$  does not Granger-cause time series  $p$ , if and only if for all  $k$ ,  $A_{p,q}^{(k)} = 0$ . To better represent nonlinear dynamics amongst time series, a nonlinear autoregressive model (NAR) (Billings, 2013)  $g$  may be defined, in which

$$x_t = g(x_{1<t}, \dots, x_{n<t}) + e_t$$

where  $x_{p< t} = (x_{p_1}, \dots, x_{p_{t-1}}, x_{p_t})$  describes the past of series  $p$ . The full nonlinear functions from the NAR are commonly modeled jointly using neural networks.

Using Granger causality as is overwhelms the generator with too much information resulting in convergence issues for the GAN. Instead of looking at traces comprehensively, we need a way to *scope* how the generator understands relationships between time series. To this end, we would like to use the same intuition developed from Granger causality, namely developing an understanding of relationships comprehensively using less stringent temporal constraints, but scope these relationships specifically in terms of *motifs*. Therefore, we develop a concept of *motif causality* which, by learning causal relationships amongst sequences of motifs, allows the generator to learn realistic motif sequences and produce high quality synthetic traces as a result.

## 4. Motif Causality

### 4.1. Extending Granger Causality to Motifs

In order to quantify the relationships amongst sequences of motifs to best capture glucose dynamics, we extend the idea of Granger causality to work with motifs, which we denote as *motif causality*. Given a motif set with  $m$  motifs, we build a separate (component) model, a so-called **motif network** in our model, for *each* motif. For a single motif  $\mu_i$  at time  $t$ ,  $\mu_{i,t}$ , we define a function  $g_i$  specifying how motifs in previous timesteps are mapped to that motif

$$\mu_{i,t} = g_i(\mu_{1<t}, \dots, \mu_{n<t}) + e_{i,t}$$

where  $\mu_{j< t} = (\mu_{j_1}, \dots, \mu_{j_{t-1}}, \mu_{j_t})$  describes the past of motif  $\mu_j$ .  $g_i$  outputs a vector and  $e_{i,t}$  is a vector. Essentially, we define motif  $\mu_i$  in terms of its relationship to past motifs.

A  $g_i$  function for each motif  $\mu_i$  in the motif set is implemented via a motif network with a single-layer RNN architecture. In the RNN, the historical context of the series for predicting a component motif  $\mu_i$  is represented by the  $H$ -dimensional hidden state at time  $t$ :  $h_t \in \mathbb{R}^H$ . At time  $t$ , the hidden state is updated:

$$h_t = g_i(h_{t-1}) + e_{i,t}$$

and  $g_i$  is modeled as a single-layer LSTM as they are good at modeling long, nonlinear dependencies amongst traces (Yu et al., 2019). As such, the output for a motif  $\mu_i$  at time  $t$ ,  $\mu_{i,t}$ , can be obtained by a linear decoding of the hidden state:

$$\mu_{i,t} = W^o h_t + e_{i,t}$$

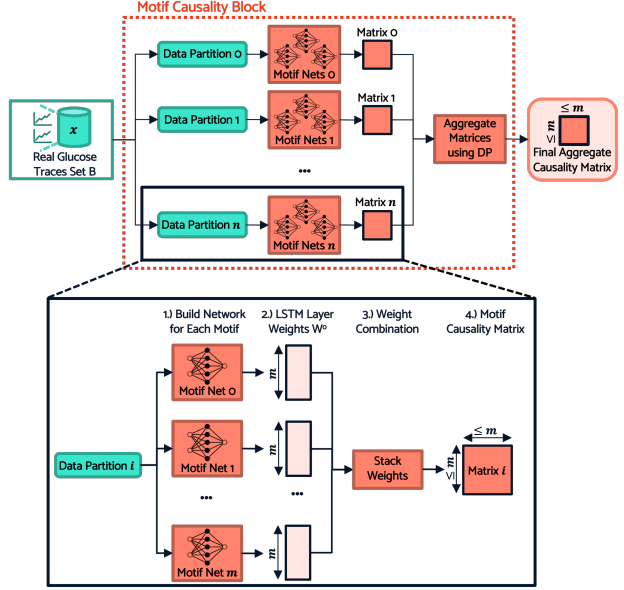


Figure 3. Motif Causality Block. The highlighted bottom box shows the zoomed-in steps that occur within each data partition.

where  $W^o$  is a matrix of the output weights. These weights control the update of the hidden state and thereby control the influence of past motifs on this component motif. If all elements in the  $j$ th column of  $W^o$  are zero,  $W_{:,j}^o = 0$ , this is a sufficient condition for an input motif  $\mu_j$  being motif non-causal on an output  $\mu_i$ . Therefore, we can find the motifs that are motif-causal of motif  $\mu_i$  using a group lasso penalty optimization across the columns of  $W^o$ :

$$\min_W \sum_{t=2}^T (\mu_{i,t} - g_i(\mu_{0<t}, \dots, \mu_{n<t}))^2 + \sum_{j=1}^n \|W_{:,j}^o\|_2$$

We define this as the local motif loss  $\mathcal{L}_{ml}$ , optimized in each motif net using proximal gradient descent.

### 4.2. Training Within A Data Partition

Figure 3 shows the overall architecture of the motif causality block. We next describe how training occurs within each data partition (Steps 1-4 in zoomed part of Fig. 3), and then explain how the block is trained as a whole in Section 4.3.

**Build a Motif Network for Each Motif.** As a pre-processing step, we assume each time series trace has been chunked into a sequence of motifs of specified size  $\tau$  (see Section 3.1 for more details).  $\tau$  is a model hyperparameter, which we suggest chosen based on the longest effect time of a trace event. We use  $\tau = 48$ , corresponding to 4 hours of time, because most large glucose events (from behaviors like eating) are encompassed within that time frame. To model motif causality for an entire set of data, a  $g_i$  function is implemented for each motif via a separate RNN motif network following the description provided previously, resulting in  $m$  total networks (Step 1, Fig. 3).



**Combining Outputs of Individual Motif Networks.** Each motif network outputs a matrix of weights  $W^o$  corresponding to the learned causal relationships (Step 2, Fig. 3). Values in the matrix are between 0 and 1 and give the degree to which every other motif is motif causal of the particular motif  $\mu_i$  the RNN was specialized for. 0 indicates no causal relationship and 1 indicates the strongest relationship (an example is in Fig. 7 in the Appendix). To return a complete matrix that summarizes causal relationships amongst *all* motifs, we stack the weights (Step 3, Fig. 3) and return a complete  $m \times m$  motif causality matrix (Step 4, Fig. 3).

#### 4.3. Training the Entire Motif Causality Block

The entire motif causality block, displayed in Fig. 3, is trained in a private way using differential privacy (DP).

**Differential Privacy.** Differential Privacy (Dwork, 2008) is a formal definition of privacy that provides an intuitive bound on the amount of information that can be learned about any individual in a dataset. DP is defined formally as follows: A randomized algorithm  $\mathcal{M}$  satisfies  $(\epsilon, \delta)$ -differential privacy if, for all datasets  $D_1$  and  $D_2$  differing by at most a single element, and all  $S \subseteq \text{Range}(\mathcal{M})$ ,

$$\Pr[\mathcal{M}(D_1) \in S] \leq e^\epsilon \Pr[\mathcal{M}(D_2) \in S] + \delta$$

$(\epsilon, \delta)$  are important privacy parameters determining the *privacy budget*, which dictates the level of privacy guaranteed by the algorithm; smaller values indicate stronger privacy.

**Partition Data.** A separate dataset from the one used to train the rest of the GAN must be used for the motif causality block, so that our privacy budget does not need to be shared between the two, allowing for a better privacy vs. utility balance. We train the motif causality block using a PATE framework (Papernot et al., 2018). Specifically, the data is partitioned into  $n$  partitions based on the privacy budget  $(\epsilon, \delta)$  such that no models are trained on overlapping data.

**Train Motif Networks.** The set of motif networks are trained within each data partition following the procedure described previously (Section 4.2). The output of each data partition is a motif causality matrix, resulting in  $n$  total matrices, each of dimensionality  $m \times m$ . The partitions are trained in parallel to speed up training time.

**Aggregate Motif Causality Matrices.** In the PATE framework, carefully calibrated noise is added to a histogram of votes for each class, such that the classes with the noisiest votes are outputted. Relatedly, each value in a motif causality matrix may be likened to a class (e.g., causal prediction between motif  $\mu_i$  and  $\mu_j$ ); therefore, we use this mechanism to aggregate the weights in the matrices and return the final aggregate causality matrix,  $M$ , (more details in (Papernot et al., 2018)). With DP, noise is tuned based on the privacy budget, implemented using the Tensorflow Privacy library; otherwise, we aggregate the matrices without any noise.

**Integration with GAN.** The final causality matrix,  $M$  is sent to the generator to help it learn how to conserve motif relationships within sequences of motifs in the synthetically generated data. Details are described next in Section 5.2.

## 5. Complete GlucoSynth Framework

The GlucoSynth framework is shown in Figure 4, and consists of four key blocks: an autoencoder, the motif causality block, a generator and a discriminator. Two completely separate datasets are used for the training of the motif causality block and the GAN. This allows us to use *separate* privacy budgets when training each part, resulting in a better privacy vs. utility tradeoff since the budget does not need to be shared. We walk through each component of the GAN next.

### 5.1. Autencoder

We use an autoencoder (AE) with an RNN architecture to learn a lower dimensional representation of the traces, allowing the generator to better preserve underlying temporal dynamics of the traces. The autoencoder consists of two networks: an embedder and a recovery network. The embedder uses an encoding function to map the real data into a lower dimensional space:  $Enc(x) : x \in \mathbb{R}^n \rightarrow x_e \in \mathbb{R}^e$  while the recovery network reverses this process, and uses a decoding function to map the embedded data back to the original dimensional space:  $Dec(x_e) : x_e \in \mathbb{R}^e \rightarrow \tilde{x} \in \mathbb{R}^n$ . A foolproof autoencoder perfectly reconstructs the original input data, such that  $x = \tilde{x}$ . This process yields the Reconstruction Loss,  $\mathcal{L}_R$ , the Mean Square Error (MSE) between the original data  $x$  and the recovered data,  $\tilde{x}$ :  $\text{MSE}(x, \tilde{x})$ .

### 5.2. Generator

We implement the generator via an RNN or LSTM. Importantly, the generator works in the embedded space, by receiving the input traces passed through the embedder ( $x_e$ ). To generate synthetic data, a random vector of noise,  $z$  is passed through the generator and then the recovery network to return the synthetic traces in the original dimensional space. To learn how to produce high-quality synthetic data, the generator receives three key pieces of information:

**1 - Stepwise.** First, the generator receives batches of real data to guide the generation of realistic next step vectors. To do this, a Stepwise Loss,  $\mathcal{L}_S$  is computed at time  $t$  using the MSE between the batch of embedded real data,  $x_{et}$ , and the batch of embedded synthetic data,  $\hat{x}_{et}$ :  $\text{MSE}(x_{et}, \hat{x}_{et})$ . In this way, the generator can compare (and learn to correct) the discrepancies in stepwise data distributions.

**2 - Motif Causality.** Second, the generator needs to preserve sequences of motifs in addition to temporal dynamics. Using the aggregate causality matrix  $M$  returned from the Motif Causality Block, the generator computes a motif

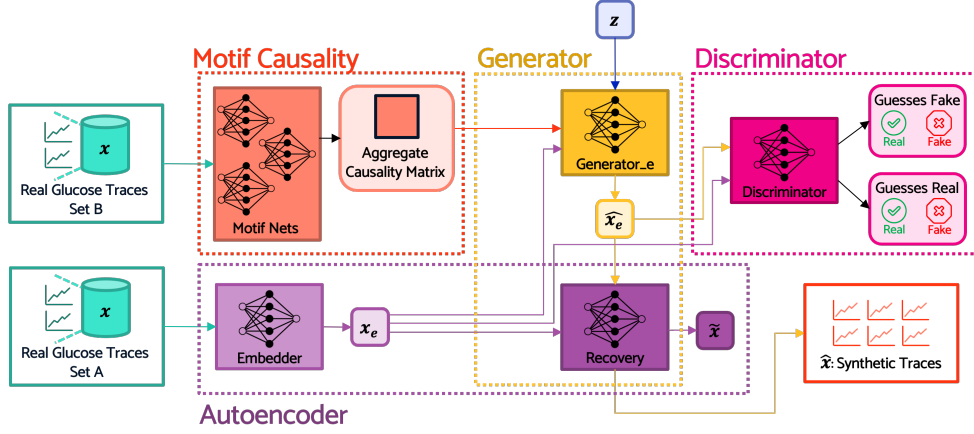


Figure 4. Overview of Complete GlucoSynth architecture.

causality matrix,  $M_{\hat{x}}$ , on the set of synthetic data  $\hat{x}$ . Because the original causality matrix was not trained on data in the embedded space, we first run the set of embedded synthetic data through the recovery network  $\hat{x}_e \rightarrow \hat{x}$ . From there, the Motif Causality Loss,  $\mathcal{L}_M$ , may be computed, the error between the two matrices using MSE:  $\text{MSE}(M, M_{\hat{x}})$ . Practically, these matrices give a causal value of seeing a motif  $\mu_i$  in the future after some motif  $\mu_j$ . Unrealistic motif sequences will have causal values close to 0 in the real matrix. As such, as the generator learns to generate synthetic data that yields a realistic causal matrix (thereby identifying appropriate causal relationships from the motifs), it implicitly learns to not generate unrealistic motif sequences.

**3 - Distributional.** Third, to guide the generator to produce a diverse set of traces, the generator computes a Distributional Loss,  $\mathcal{L}_D$ , the moments loss (MML), between the overall distribution of the real data  $x_e$  and the distribution of the synthetic data  $\hat{x}_e$ :  $\text{MML}(x_e, \hat{x}_e)$ . The MML is the difference in the mean and variance of two matrices.

### 5.3. Discriminator

The discriminator is a traditional discriminator model using an RNN architecture, the only change being it also works in the embedded space. The discriminator yields the Adversarial Loss Real,  $\mathcal{L}_{Ar}$ , the Binary Cross Entropy (BCE) between the discriminator guesses on the real data  $y_{x_e}$  and the ground truth  $y$ , a vector of 0's,  $\text{BCE}(y_{x_e}, y)$  and the Adversarial Loss Fake,  $\mathcal{L}_{Af}$ , the BCE between the discriminator guesses on the fake data  $y_{\hat{x}_e}$  and the ground truth  $y$ , a vector of 1's,  $\text{BCE}(y_{\hat{x}_e}, y)$ .

### 5.4. Privacy

Two completely separate datasets are used for the training of the motif causality block and the GAN, allowing us to use *separate* privacy budgets for each, resulting in a better privacy-utility tradeoff. As a reminder, privacy has already been integrated into the motif causality block since it is

trained using a PATE framework (see Section 4.3). To add differential privacy to the rest of the GAN, each of the networks (embedder, recovery, generator, discriminator) are trained with noise added to the weights based on the specified privacy budget  $(\epsilon, \delta)$ . We use the Tensorflow Privacy DP Keras Adam Optimizer that implements the DP-SGD algorithm from (Abadi et al., 2016).

### 5.5. Overall GAN Training Procedure

First, the motif causality block is trained following the procedure described in Section 4.3, and then the rest of the GAN is trained. The autoencoder is optimized following  $\min \mathcal{L}_R + \alpha \mathcal{L}_S$ , where  $\alpha$  is a hyperparameter that balances the two loss functions. If the AE only receives  $\mathcal{L}_R$  (as typically done), it becomes overspecialized, i.e., it becomes too good at learning the *best* lower dimensional representation of the data such that the embedded data are no longer helpful to the generator. For this reason, the AE also receives  $\mathcal{L}_S$ , enabling the dual training of the generator and embedder. The generator is optimized using  $\min(1 - \mathcal{L}_{Af}) + \eta \mathcal{L}_S + \eta \mathcal{L}_D + \mathcal{L}_M$ , where  $\eta$  is a hyperparameter that balances the effect of the stepwise and distributional loss. Finally the discriminator is optimized using the traditional adversarial feedback  $\min \mathcal{L}_{Af} + \mathcal{L}_{Ar}$ . The networks are trained in sequence (within each epoch) in the following order: autoencoder, generator then discriminator. In practice we set  $\alpha$  to 0.1 and  $\eta$  to 10, as they enable GlucoSynth to converge fastest, i.e., in the fewest epochs.

## 6. Evaluation

**Data.** 100,000 single-day glucose traces collected from Dexcom's G6 Continuous Glucose Monitors (CGMs) (Ak-turk et al., 2021) were randomly sampled across each month from January to December 2022, for a total of 1.2 million traces. Data was recorded every 5 minutes ( $T = 288$ ) and each trace was aligned temporally from 00:00 to 23:59.

**Benchmarks.** We restrict our comparison to the five most

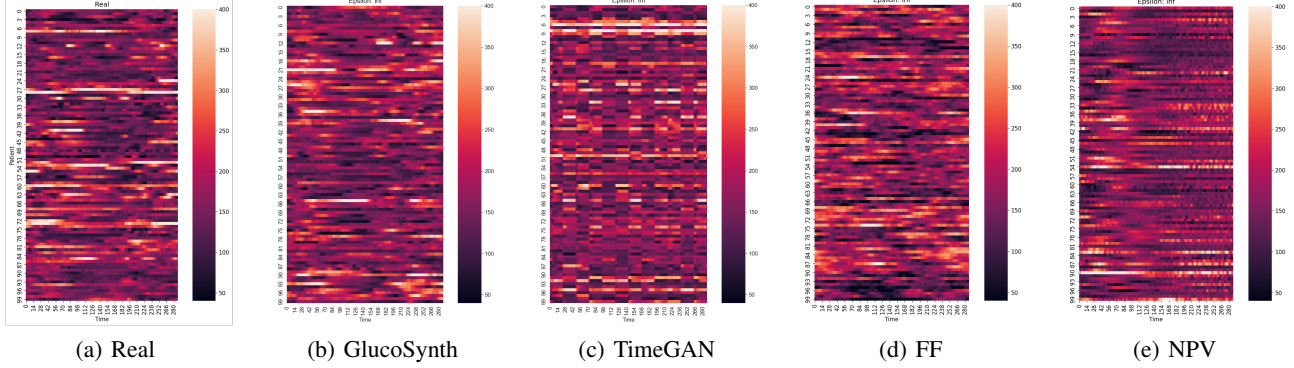


Figure 5. Heatmaps for Nonprivate Models

closely related state-of-the-art models for generating synthetic univariate time series with no labels or auxiliary data: Three nonprivate – TimeGAN (Yoon et al., 2019), Fourier Flows (FF) (Alaa et al., 2021), non-volume preserving transformations (NVP) (Dinh et al., 2016); and two private – RGAN (Esteban et al., 2017) and DPGAN (Frigerio et al., 2019). All hyperparameter settings are in Appendix B.

**Evaluation Criteria.** Evaluating synthetic data is notoriously difficult (Borji, 2022), and for this reason we provide an extensive evaluation across 3 main criteria– synthetic data should: 1) conserve characteristics of the real data (**fidelity**); 2) contain diverse patterns from the real data without the introduction of anomalous patterns (**breadth & data artifacts**); and 3) be usable in place of the original for real-world use cases (**utility**).

### 6.1. Fidelity

**Trace Visualization.** Although not a comprehensive way to evaluate synthetic data, we provide visualizations of the traces to give a snapshot view about how realistic the synthetic traces may look. Figure 5 shows a heatmap visualization of 100 randomly sampled glucose traces. Each row in the heatmap is a single trace from timestep 0 to 288, and the coloring indicates the glucose value (between 40 mg/dL and 400 mg/dL) at that timestep. Additional visuals across all models and budgets are available in Appendix C.1. As seen from the images, GlucoSynth produces realistic-looking glucose traces, even at small privacy budgets.

**Population Statistics.** To evaluate fidelity on a population scale, we compute a common set of glucose metrics for patient glycemic control and test if the difference in metrics between the synthetic and real data is statistically significant in Table 5. GlucoSynth performs the best, with few metrics with statistical differences between the real and synthetic data for  $\epsilon \geq 0.1$ . More details are in Appendix C.2.

**Distributional Comparisons.** We visualize differences in distributions between the real and synthetic data by plot-

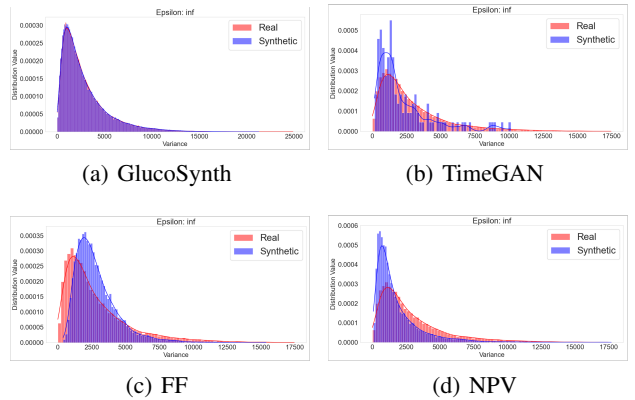


Figure 6. Distributional Variance for Nonprivate Models

ting the distribution of variances and using PCA (Bryant & Yarnold, 1995). Figure 6 and Figure 13 show the variance distribution and PCA plots, respectively, for the nonprivate models. We also compare distributions across privacy budgets: Figures 14 and 15 show GlucoSynth, Figures 16 and 17 show RGAN and Figures 18 and 19 show dpGAN. Due to space constraints, some of these figures are located in Appendix C.3. In both nonprivate and across budgets for private settings, GlucoSynth produces synthetic distributions closest to the real ones, better than all other models.

### 6.2. Breadth

We quantify breadth in terms of glucose motifs. For each model’s synthetic set of traces, we build a motif set (following the same preprocessing steps explained in Section 3.1). Given the original motif set from the real traces  $S_x$ , for each synthetic motif set  $S_{\hat{x}}$ , we compute “True Motifs”, (TM), the percentage of real motifs (motifs actually in the real motif set) in the synthetic motif set,  $TM/|S_{\hat{x}}|$ . We also compute the percentage of “Fake Motifs” (FM), motifs not contained in the real motif set,  $1 - TM$ . These metrics quantify how good our synthetic motif set is (e.g., are its motifs mostly “real” ones or are they mostly fake?) We also compute metrics related to *coverage*: how many of the total motifs in the real motif set did we find in our synthetic

Table 1. Motif Coverage. TM is true motifs, FM is fake motifs. Bolded values indicate the best ones at each privacy budget (non-private models compared with private models when  $\epsilon = \infty$ .)

Model	% TM	% FM	Coverage	MSE
GlucoSynth $\epsilon = 0.01$	<b>1.0</b>	<b>0.0</b>	0.01	<b>99.003</b>
GlucoSynth $\epsilon = 0.1$	<b>1.0</b>	<b>0.0</b>	0.083	<b>11.153</b>
GlucoSynth $\epsilon = 1$	<b>0.992</b>	<b>7.722e-3</b>	0.145	<b>6.682</b>
GlucoSynth $\epsilon = 10$	<b>1.0</b>	<b>0.0</b>	0.167	<b>5.012</b>
GlucoSynth $\epsilon = 100$	<b>0.987</b>	<b>0.013</b>	<b>0.532</b>	<b>1.622</b>
GlucoSynth $\epsilon = \infty$	<b>0.987</b>	<b>0.013</b>	<b>0.534</b>	<b>1.622</b>
TimeGAN	0.625	0.375	6.087e-3	107.702
FF	0.642	0.358	0.405	2.005
NVP	0.482	0.518	0.328	1.902
RGAN $\epsilon = 0.01$	0.013	0.987	1.391e-3	108.576
RGAN $\epsilon = 0.1$	0.015	0.985	0.031	107.291
RGAN $\epsilon = 1$	0.015	0.985	0.033	103.288
RGAN $\epsilon = 10$	0.017	0.983	0.053	100.309
RGAN $\epsilon = 100$	0.024	0.976	0.09	93.563
RGAN $\epsilon = \infty$	0.026	0.974	0.091	79.622
dpGAN $\epsilon = 0.01$	0.094	0.906	<b>0.0536</b>	180.07
dpGAN $\epsilon = 0.1$	0.39	0.61	<b>0.195</b>	28.911
dpGAN $\epsilon = 1$	0.48	0.52	<b>0.239</b>	23.171
dpGAN $\epsilon = 10$	0.743	0.257	<b>0.251</b>	16.092
dpGAN $\epsilon = 100$	0.86	0.0140	0.266	12.735
dpGAN $\epsilon = \infty$	0.855	0.145	0.293	10.914

data? We define this as  $TM/|S_x|$ . This gives a sense of the breadth in a more traditional manner. To compare actual *distributions* of motifs (not just counts), we compute the mean square error (MSE) between the distribution of real motifs  $S_x$  and the distribution of synthetic motifs  $S_{\hat{x}}$ . This gives a measure about how close the synthetic motif distribution is to the real one. We want a high % TM and coverage values and low % FM and MSE. Results are in Table 1; compared to all other models across all privacy budgets, overall our model provides the best breadth results. Additional analysis is available in Appendix D.

### 6.3. Utility

We evaluate our synthetic glucose traces for use in a glucose forecasting task using the common paradigm TSTR (Train on Synthetic, Test on Real), in which the synthetic data is used to train the model and then tested on the original data. This use case was chosen as it is a frequent real-world problem in both academic and industry scenarios (e.g., used in the current development of artificial insulin delivery.) We train a LSTM network optimized for glucose forecasting tasks (Kushner et al., 2020) and report the Root Mean Square Error (RMSE). Results are summarized in Table 2.

Since RMSE may provide a limited view about the predictions from the glucose forecasting model, we also plot the Clarke Error Grid (Clarke, 2005), which visualizes the differences between a predictive and a reference measurement, and is a basis for evaluation of the safety of diabetes-related medical devices (for example, used for evaluating glucose outputs from predictive models integrated into artificial insulin delivery systems). More details are available in Ap-

Table 2. RMSE For Glucose Forecasting using TSTR. Bolded values are the best results on the synthetic data at each privacy budget (nonprivate models compared with private models when  $\epsilon = \infty$ ).

Model	RMSE
Real (TRTR)	$7.079e-3 \pm 4.173e-3$
GlucoSynth $\epsilon = 0.01$	<b><math>0.038 \pm 2.77e-4</math></b>
GlucoSynth $\epsilon = 0.1$	<b><math>0.036 \pm 2.95e-4</math></b>
GlucoSynth $\epsilon = 1$	<b><math>0.030 \pm 1.39e-4</math></b>
GlucoSynth $\epsilon = 10$	<b><math>0.029 \pm 1.19e-4</math></b>
GlucoSynth $\epsilon = 100$	<b><math>0.029 \pm 1.83e-4</math></b>
GlucoSynth $\epsilon = \infty$	<b><math>7.787e-3 \pm 1.59e-4</math></b>
TimeGAN	$0.061 \pm 2.63e-4$
FF	$0.038 \pm 2.7e-4$
NVP	$0.029 \pm 3.4e-5$
RGAN $\epsilon = 0.01$	$0.819 \pm 9.982e-3$
RGAN $\epsilon = 0.1$	$0.688 \pm 6.283e-3$
RGAN $\epsilon = 1$	$0.651 \pm 0.018$
RGAN $\epsilon = 10$	$0.619 \pm 0.016$
RGAN $\epsilon = 100$	$0.549 \pm 0.011$
RGAN $\epsilon = \infty$	$0.460 \pm 0.013$
dpGAN $\epsilon = 0.01$	$0.205 \pm 4.637e-3$
dpGAN $\epsilon = 0.1$	$0.045 \pm 2.015e-4$
dpGAN $\epsilon = 1$	$0.03 \pm 2.338e-5$
dpGAN $\epsilon = 10$	$0.035 \pm 7.54e-5$
dpGAN $\epsilon = 100$	$0.031 \pm 5.453e-5$
dpGAN $\epsilon = \infty$	$0.028 \pm 5.41e-5$

pendix E. GlucoSynth provides the best forecasting results compared to all other models across all privacy budgets.

## 7. Limitations & Conclusion

**Limitations.** In order to train on a huge set of glucose traces, we used a private dataset that is not publicly available<sup>1</sup>. That being said, smaller samples of glucose traces with similar patient populations are available at OpenHumans<sup>2</sup> and the T1D Exchange Registry<sup>3</sup>. In addition, one of the reasons our privacy results perform well is because we use two *separate* datasets for the training of the motif causality block and the rest of the GAN. However, this may be a limiting factor for others that do not have a large set of traces available (and for instance, may need to now split their already small dataset into two separate cohorts.)

**Conclusion.** In this paper we have presented GlucoSynth, a novel GAN framework with integrated differential privacy to generate synthetic glucose traces. GlucoSynth conserves motif relationships within the traces, in addition to the typical temporal dynamics contained within time series. We also presented a comprehensive evaluation using 1.2 million

<sup>1</sup>We note that one of the motivations for this project was to share a synthetic version of these traces.

<sup>2</sup><https://www.openhumans.org/>

<sup>3</sup><https://t1dexchange.org/registry/>



glucose traces wherein our model outperformed all previous models across three criteria of fidelity, breadth and utility.

## References

- Abadi, M., Chu, A., Goodfellow, I., McMahan, H. B., Mironov, I., Talwar, K., and Zhang, L. Deep learning with differential privacy. In *Proceedings of the 2016 ACM SIGSAC conference on computer and communications security*, pp. 308–318, 2016.
- Akturk, H. K., Dowd, R., Shankar, K., and Derdzinski, M. Real-world evidence and glycemic improvement using dexcom g6 features. *Diabetes Technology & Therapeutics*, 23(S1):S–21, 2021.
- Alaa, A., Chan, A. J., and van der Schaar, M. Generative time-series modeling with fourier flows. In *International Conference on Learning Representations*, 2021.
- Alcaraz, J. M. L. and Strodthoff, N. Diffusion-based time series imputation and forecasting with structured state space models. *arXiv preprint arXiv:2208.09399*, 2022.
- Billings, S. A. *Nonlinear system identification: NARMAX methods in the time, frequency, and spatio-temporal domains*. John Wiley & Sons, 2013.
- Binanay, C., Califf, R. M., Hasselblad, V., O’Connor, C. M., Shah, M. R., Sopko, G., Stevenson, L. W., Francis, G. S., Leier, C. V., Miller, L. W., et al. Evaluation study of congestive heart failure and pulmonary artery catheterization effectiveness: the escape trial. *Jama*, 294(13):1625–1633, 2005.
- Borji, A. Pros and cons of gan evaluation measures: New developments. *Computer Vision and Image Understanding*, 215:103329, 2022.
- Britton, K. E. and Britton-Colonnese, J. D. Privacy and security issues surrounding the protection of data generated by continuous glucose monitors. *Journal of diabetes science and technology*, 11(2):216–219, 2017.
- Brophy, E., Wang, Z., She, Q., and Ward, T. Generative adversarial networks in time series: A survey and taxonomy. *arXiv preprint arXiv:2107.11098*, 2021.
- Bryant, F. B. and Yarnold, P. R. Principal-components analysis and exploratory and confirmatory factor analysis. *American Psychological Association*, 1995.
- Clarke, W. L. The original clarke error grid analysis (ega). *Diabetes technology & therapeutics*, 7(5):776–779, 2005.
- Dinh, L., Sohl-Dickstein, J., and Bengio, S. Density estimation using real nvp. *arXiv preprint arXiv:1605.08803*, 2016.
- Dogariu, M., Ștefan, L.-D., Boteanu, B. A., Lamba, C., Kim, B., and Ionescu, B. Generation of realistic synthetic financial time-series. *ACM Transactions on Multimedia Computing, Communications, and Applications (TOMM)*, 18(4):1–27, 2022.
- Dwork, C. Differential privacy: A survey of results. In *International conference on theory and applications of models of computation*, pp. 1–19. Springer, 2008.
- Esteban, C., Hyland, S. L., and Rätsch, G. Real-valued (medical) time series generation with recurrent conditional gans. *arXiv preprint arXiv:1706.02633*, 2017.
- Frigerio, L., Oliveira, A. S. d., Gomez, L., and Duverger, P. Differentially private generative adversarial networks for time series, continuous, and discrete open data. In *IFIP International Conference on ICT Systems Security and Privacy Protection*, pp. 151–164. Springer, 2019.
- Goodfellow, I., Pouget-Abadie, J., Mirza, M., Xu, B., Warde-Farley, D., Ozair, S., Courville, A., and Bengio, Y. Generative adversarial networks. *Communications of the ACM*, 63(11):139–144, 2020.
- Granger, C. W. Investigating causal relations by econometric models and cross-spectral methods. *Econometrica: journal of the Econometric Society*, pp. 424–438, 1969.
- Hazra, D. and Byun, Y.-C. Synsiggan: Generative adversarial networks for synthetic biomedical signal generation. *Biology*, 9(12):441, 2020.
- Jordon, J., Yoon, J., and Van Der Schaar, M. Pate-gan: Generating synthetic data with differential privacy guarantees. In *International conference on learning representations*, 2018.
- Kushner, T., Breton, M. D., and Sankaranarayanan, S. Multi-hour blood glucose prediction in type 1 diabetes: A patient-specific approach using shallow neural network models. *Diabetes Technology & Therapeutics*, 22(12): 883–891, 2020.
- Li, X., Metsis, V., Wang, H., and Ngu, A. H. H. Tts-gan: A transformer-based time-series generative adversarial network. In Michalowski, M., Abidi, S. S. R., and Abidi, S. (eds.), *Artificial Intelligence in Medicine*, pp. 133–143. Cham, 2022. Springer International Publishing.
- Lin, Z., Jain, A., Wang, C., Fanti, G., and Sekar, V. Using gans for sharing networked time series data: Challenges, initial promise, and open questions. In *Proceedings of the ACM Internet Measurement Conference*, pp. 464–483, 2020.
- Lütkepohl, H. *New introduction to multiple time series analysis*. Springer Science & Business Media, 2005.

- Ni, H., Szpruch, L., Wiese, M., Liao, S., and Xiao, B. Conditional sig-wasserstein gans for time series generation. *arXiv preprint arXiv:2006.05421*, 2020.
- Papernot, N., Song, S., Mironov, I., Raghunathan, A., Talwar, K., and Erlingsson, Ú. Scalable private learning with pate. *arXiv preprint arXiv:1802.08908*, 2018.
- Razghandi, M., Zhou, H., Erol-Kantarci, M., and Turgut, D. Variational autoencoder generative adversarial network for synthetic data generation in smart home. *arXiv preprint arXiv:2201.07387*, 2022.
- Torfi, A., Fox, E. A., and Reddy, C. K. Differentially private synthetic medical data generation using convolutional gans. *Information Sciences*, 586:485–500, 2022.
- Xie, L., Lin, K., Wang, S., Wang, F., and Zhou, J. Differentially private generative adversarial network. *arXiv preprint arXiv:1802.06739*, 2018.
- Yoon, J., Jarrett, D., and Van der Schaar, M. Time-series generative adversarial networks. *Advances in neural information processing systems*, 32, 2019.
- Young-Hyman, D., De Groot, M., Hill-Briggs, F., Gonzalez, J. S., Hood, K., and Peyrot, M. Psychosocial care for people with diabetes: a position statement of the american diabetes association. *Diabetes care*, 39(12):2126–2140, 2016.
- Yu, Y., Si, X., Hu, C., and Zhang, J. A review of recurrent neural networks: Lstm cells and network architectures. *Neural computation*, 31(7):1235–1270, 2019.

Table 3. Summary of Previous Methods for Time Series Synthesis. \*CI = conditional information or extra features

Name	Private?	No Labels Required?	No CI*?	Length
TimeGAN (Yoon et al., 2019)	x	✓	✓	24 - 58
TTS-GAN (Li et al., 2022)	x	x	✓	24 - 150
SigCWGAN (Ni et al., 2020)	x	✓	x	80,000
RGAN (Esteban et al., 2017)	✓	✓	✓	16 - 30
RCGAN (Esteban et al., 2017)	✓	✓	x	16 - 30
dpGAN (Frigerio et al., 2019)	✓	✓	✓	96
RDP-CGAN (Torfi et al., 2022)	✓	✓	x	2 - 4097
DoppelGANger (Lin et al., 2020)	✓	✓	x	50 - 600
Glucosynth (Ours)	✓	✓	✓	288+

## A. Extended Related Work

We overview related work in three lines of research: time series, conditional time series, and time series methods that employ differential privacy. Table 3 summarizes previous time series synthesis methods. We note that there have been exciting developments for adjacent research tasks (data augmentation, forecasting) such as diffusion models (Alcaraz & Strodtzoff, 2022), but there are not yet any publicly available models specifically for the generation of complete synthetic time series datasets. As such, we focus the scope of our comparison on the current state-of-the-art methods for synthetic time series which all build upon Generative Adversarial Networks (GANs) (Goodfellow et al., 2020) and transformation-based approaches (Dinh et al., 2016). In particular TimeGAN (Yoon et al., 2019), RGAN (Esteban et al., 2017) and dpGAN (Frigerio et al., 2019) are most similar to ours and used as benchmarks in the evaluation in Section 6.

**Time Series.** There have been promising models to generate synthetic time series across a variety of domains such as financial data (Dogariu et al., 2022), cyber-physical systems (e.g., smart homes (Razghandi et al., 2022)), and medical signals (Hazra & Byun, 2020). Brophy et al. (2021) provides a survey of GANs for time series synthesis. TimeGan (Yoon et al., 2019) is a popular benchmark that jointly learns an embedding space using supervised and adversarial objectives in order to capture the temporal dynamics amongst traces. TTS-GAN (Li et al., 2022), trains a GAN model that uses a transformer encoding architecture in order to best preserve temporal dynamics. Transformation-based approaches have also had success for time series data. Real-valued non-volume preserving transformations (NVP) (Dinh et al., 2016) model the underlying distribution of the real data using generative probabilistic modeling and use this model to output a set of synthetic data. Similarly, Fourier Flows (FF) (Alaa et al., 2021) transform input traces into the frequency domain and output a set of synthetic data from the learned spectral representation of the original data. Methods that only focus on learning the temporal or distributional dynamics in time series are not sufficient for generating *realistic* synthetic glucose traces due to the lack of temporal dependence within sequences of glucose motifs.

**Conditional Time Series.** Many works have developed time series models that supplement their training using extra features or conditional data. Esteban et al. (2017) develops two GAN models (RGAN/RCGAN) with RNN architectures, conditioned on auxiliary information provided at each timestep during training. SigCWGAN (Ni et al., 2020) uses a mathematical conditional metric ( $Sig - W_1$ ) characterizing the signature of a path to capture temporal dependence of joint probability distributions in long time series data. However, our glucose traces do not have any additional information available so these methods cannot be used<sup>4</sup>.

**Differentially-Private GANs.** To protect sensitive data, several GAN architectures (DP GANs) have been designed to incorporate privacy-preserving noise needed to satisfy differential privacy guarantees (Xie et al., 2018). Although DP GANs such as PateGAN (Jordon et al., 2018) have had great success for other data types and learning tasks (e.g., tabular data, supervised classification tasks), results have been less satisfactory in DP GANs developed for time series.

RGAN/RCGAN (Esteban et al., 2017) also includes a DP implementation, but the authors find large gaps in performance between the nonprivate and private models. Frigerio et al. (2019) extends a simple DP GAN architecture (denoted dpGAN) to time-series data. The synthetic data from their private model conserves the distribution of the real data but loses some of the variability (diversity) from the original samples. RDP-CGAN (Torfi et al., 2022) develops a convolutional GAN architecture that uses Rényi differential privacy specifically for medical data. Across different datasets, they find that

<sup>4</sup>There is a caveat here that RGAN does not use auxiliary information, hence why we compare with it in our benchmarks.

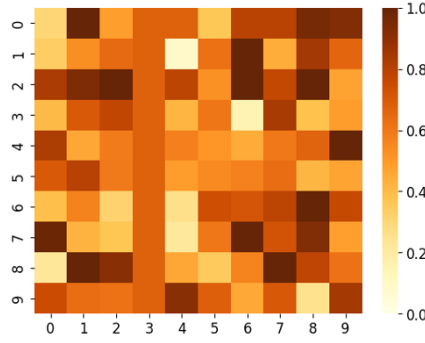


Figure 7. Example motif causality matrix for a small motif set ( $m = 10$ ). Each value in the grid is between 0 and 1. 0 indicates no motif-causal relationship, and 1 indicates the strongest motif causal relationship.

reasonable privacy budgets result in major drops in the performance of the synthetic data. Finally, DoppelGANger (Lin et al., 2020) develops a temporal GAN framework for time series with metadata and perform an in-depth privacy evaluation. Notably, they find that providing strong theoretical DP guarantees results in destroying the fidelity of the synthetic data, beyond anything feasible for use in real-world scenarios. Each of these methods touches on the innate challenge of generating DP synthetic time series due to very high tradeoffs between utility and privacy. Our DP framework uses two different methods to integrate privacy into our GAN architecture, resulting in a better utility-privacy trade-off than previous methods.

## B. Additional Experimental Details

**Note on Data Use.** As explained in the approach (Section 5), our model uses two *separate* datasets for the training of the motif causality block and the rest of the GAN. As such, we used two different samples of glucose traces with no overlap between patients for the training of each section (meaning we actually used a total of 2.4 million traces across the entire model).

**Extra Benchmark Details.** TimeGAN (Yoon et al., 2019) is implemented from [www.github.com/jsyoon0823/TimeGAN](https://www.github.com/jsyoon0823/TimeGAN); Fourier Flows (FF) (Alaa et al., 2021) are implemented from [www.github.com/ahmedmalaa/Fourier-flows](https://www.github.com/ahmedmalaa/Fourier-flows); RGAN (Esteban et al., 2017) is implemented from [www.github.com/ratschlab/RGAN](https://www.github.com/ratschlab/RGAN); and DPGAN (Frigerio et al., 2019) is adapted from [www.github.com/SAP-samples/security-research-differentially-private-generative-models](https://www.github.com/SAP-samples/security-research-differentially-private-generative-models).

**Hyperparameters.** Throughout all our experiments we use a motif tolerance  $\sigma = 2$  mg/dL, motif length  $\tau = 48$ , and GlucoSynth model parameters of  $\alpha = 0.1$  and  $\eta = 10$ . There are  $m = 5,977,610$  total motifs in the motif set. We vary  $\epsilon$  in our privacy experiments, but keep  $\delta$  the same at  $5e-4$ . All the benchmarks were trained according to their suggested parameters, with most models trained for 10,000 epochs. We note that we trained for more than the suggested epochs (50,000 instead of 10,000) and tried many additional hyperparameter settings for RGAN to attempt to improve its performance and provide the fairest comparison possible. Our experiments were completed in the Google Cloud platform on an Intel Skylake 96-core cpu with 360 GB of memory.

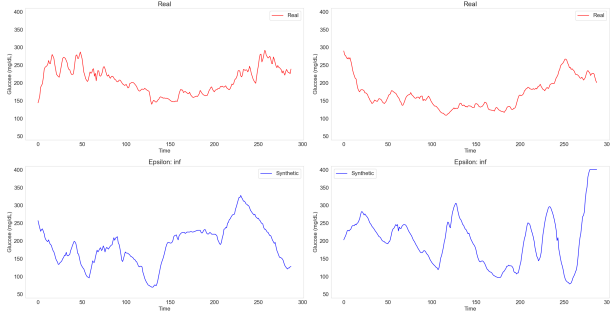
## C. Additional Evaluation: Fidelity

### C.1. Visualizations

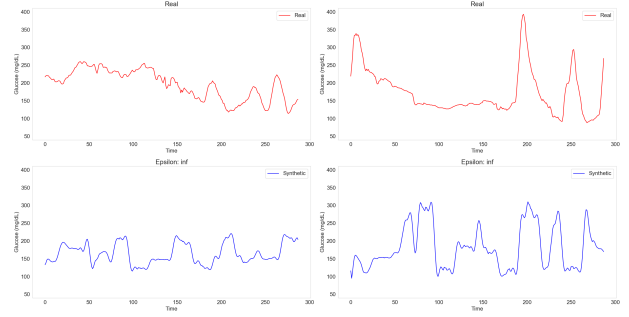
**Traces.** We provide visualizations of sample real and synthetic glucose traces from all the models. Although this is not a comprehensive way to evaluate trace quality, it does give a snapshot view about what synthetic traces may look like. Figure 8 shows randomly sampled individual traces across the nonprivate models, and Figure 9 shows traces across different privacy budgets for the private models. As evidenced by the figures, GlucoSynth produces highly realistic synthetic glucose traces, even at small privacy budgets.



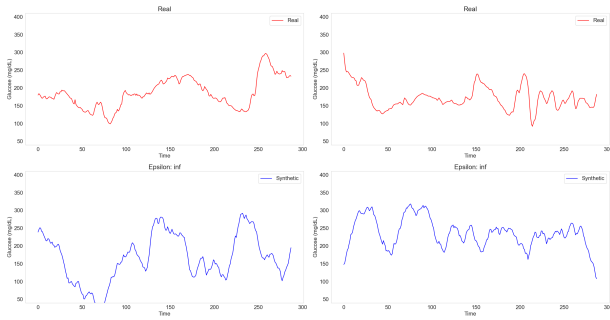
## GlucoSynth: Generating Differentially-Private Synthetic Glucose Traces



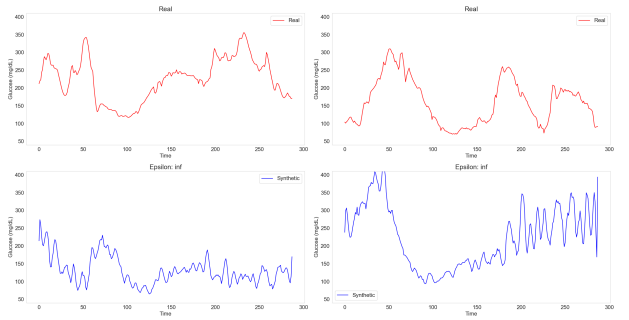
(a) GlucoSynth



(b) TimeGAN

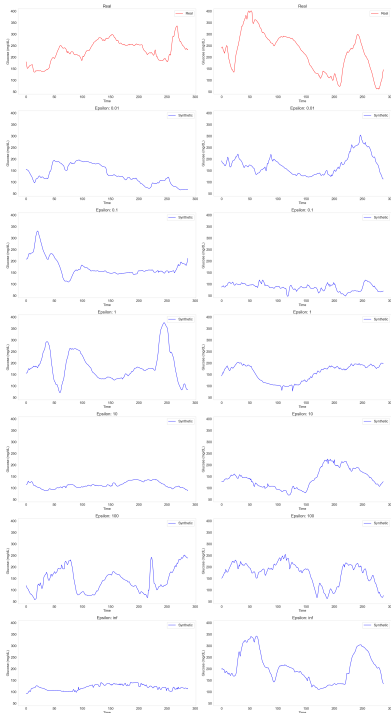


(c) FF

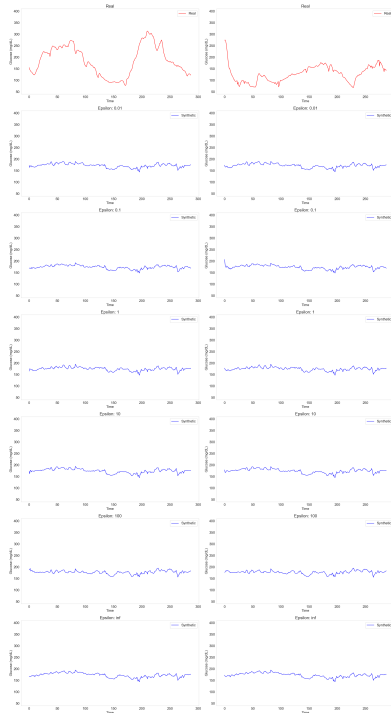


(d) NPV

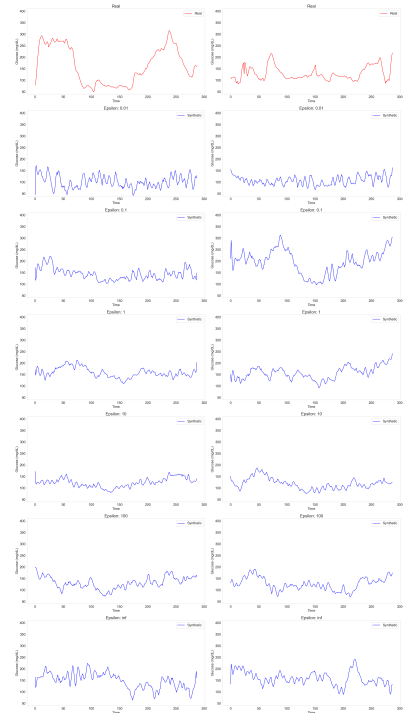
Figure 8. Sample Traces for Nonprivate Models



(a) GlucoSynth



(b) RGAN



(c) dpGAN

Figure 9. Sample Traces for Private Models Across Privacy Budgets

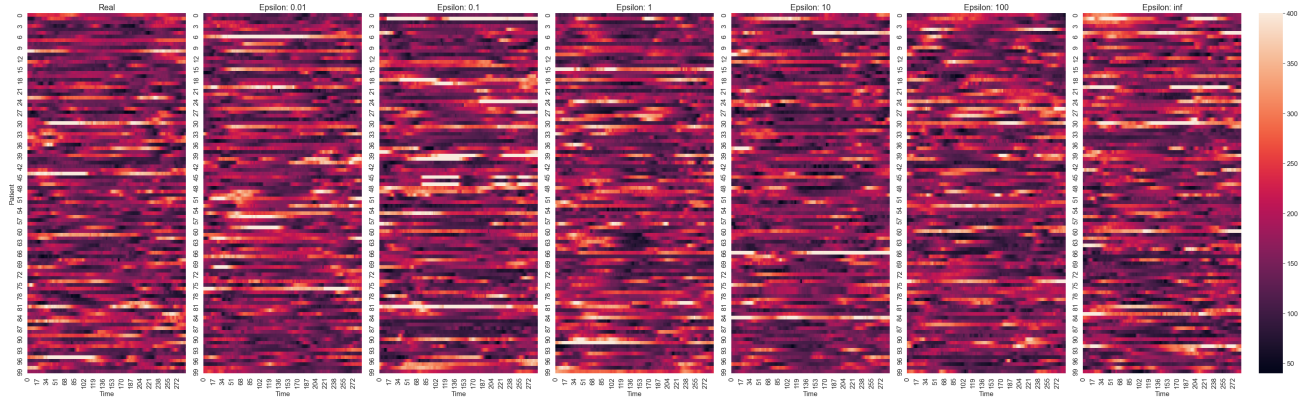


Figure 10. Heatmaps for GlucoSynth Across Different Privacy Budgets

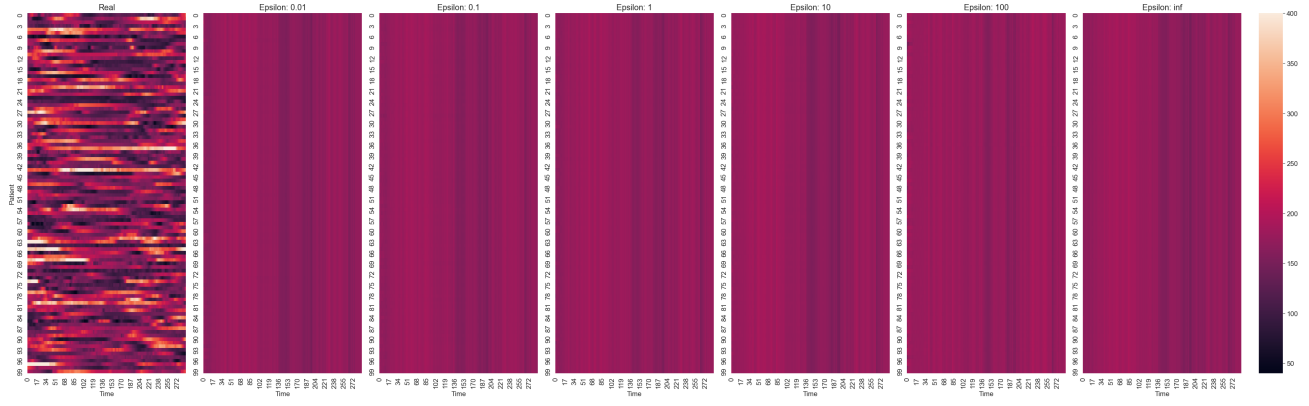


Figure 11. Heatmaps for RGAN Across Different Privacy Budgets

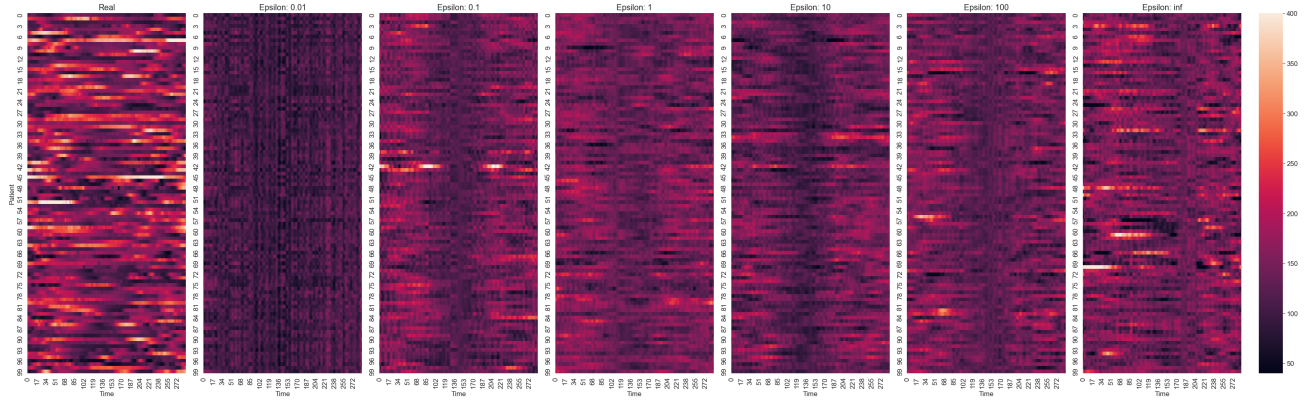


Figure 12. Heatmaps for dpGAN Across Different Privacy Budgets

**Heatmaps.** We also provide a heatmap visualization of the traces, to give a slightly larger snapshot view of the outputted synthetic vs real traces. Each heatmap contains 100 randomly sampled glucose traces. Each row is a single trace from timestep 0 to 288. The values in each row indicate the glucose value (between 40 mg/dL and 400 mg/dL). Figure 5 in the main text shows the nonprivate models, and Figures 10, 11, 12 show the private models with different privacy budgets. Upon examining the heatmaps, we notice that GlucoSynth consistently generates realistic looking glucose traces, even at very small privacy budgets.

Table 4. Glycemic Metric Explanations

Metric	Name	Explanation
VAR	Signal Variance	average trace variability
TIR	Time in Range	% of time glucose $\geq 70$ & $\leq 180$
Hypo	Time Hypoglycemic	% of time glucose $< 70$
Hyper	Time Hyperglycemic	% of time glucose $> 180$
GVI	Glycaemic Variability Index	more detailed measure of glucose variability
PGS	Patient Glycaemic Status	metric combining GVI and TIR

Table 5. Population Data Statistics. Each cell value for the synthetic data shows the (metric, p-value) using a 0.05 testing threshold. Bolded values do not have a statistically significant difference from the real data (what we want).

Model	VAR	TIR	Hypo	Hyper	GVI	PGS
Real Data	2832.76	60.31	1.58	38.11	4.03	349.23
GlucoseSynth $\epsilon = 0.01$	2575.501, 0.0	61.759, $2.0e-5$	1.331, 0.0	36.91, $5.66e-4$	<b>4.002, 0.085</b>	323.056, 0.0
GlucoseSynth $\epsilon = 0.1$	<b>2803.513, 0.356</b>	<b>60.088, 0.532</b>	1.264, 0.0	<b>38.648, 0.137</b>	$3.969, 2.74e-4$	<b>347.562, 0.712</b>
GlucoseSynth $\epsilon = 1$	2760.853, 0.022	<b>60.597, 0.41</b>	<b>1.512, 0.163</b>	<b>37.892, 0.537</b>	<b>4.019, 0.577</b>	<b>345.159, 0.368</b>
GlucoseSynth $\epsilon = 10$	<b>2800.805, 0.316</b>	<b>60.24, 0.845</b>	<b>1.538, 0.395</b>	<b>38.222, 0.76</b>	$3.963, 6.7e-5$	<b>344.376, 0.28</b>
GlucoseSynth $\epsilon = 100$	<b>2796.424, 0.244</b>	<b>60.138, 0.625</b>	<b>1.567, 0.808</b>	<b>38.295, 0.609</b>	<b>4.044, 0.32</b>	<b>352.679, 0.449</b>
GlucoseSynth $\epsilon = \infty$	<b>2811.622, 0.503</b>	<b>60.165, 0.682</b>	<b>1.54, 0.416</b>	<b>38.295, 0.61</b>	<b>4.056, 0.083</b>	<b>353.584, 0.339</b>
TimeGAN	$2234.576, 8.08e-3$	<b>62.315, 0.42</b>	$0.657, 8.233e-3$	<b>37.028, 0.669</b>	5.482, 0.0	$503.148, 0.2e-5$
FF	<b>2836.067, 0.902</b>	46.578, 0.0	5.627, 0.0	47.795, 0.0	4.931, 0.0	528.773, 0.0
NVP	1789.430, 0.0	65.499, 0.0	<b>1.507, 0.154</b>	32.994, 0.0	6.607, 0.0	589.473, 0.0
RGAN $\epsilon = 0.01$	56.96, 0.0	78.756, 0.0	0.0, $1.78e-4$	21.244, 0.0	2.52, 0.0	93.409, 0.0
RGAN $\epsilon = 0.1$	52.553, 0.0	$71.617, 3.7e-5$	0.0, $1.78e-4$	25.715, 0.0	2.208, 0.0	98.944, 0.0
RGAN $\epsilon = 1$	67.346, 0.0	78.154, 0.0	0.0, $1.78e-4$	21.846, 0.0	2.251, 0.0	85.417, 0.0
RGAN $\epsilon = 10$	76.632, 0.0	83.681, 0.0	0.0, $1.78e-4$	16.319, 0.0	2.23, 0.0	64.562, 0.0
RGAN $\epsilon = 100$	84.918, 0.0	74.285, 0.0	0.0, $1.78e-4$	$25.715, 0.6e-5$	2.208, 0.0	98.944, 0.0
RGAN $\epsilon = \infty$	89.702, 0.0	78.044, 0.0	0.0, $1.78e-4$	21.956, 0.0	2.184, 0.0	82.923, 0.0
dpGAN $\epsilon = 0.01$	451.098, 0.0	95.275, 0.0	4.60, 0.0	0.124, 0.0	7.718, 0.0	41.549, 0.0
dpGAN $\epsilon = 0.1$	1057.205, 0.0	86.43, 0.0	0.837, 0.0	12.732, 0.0	6.349, 0.0	148.412, 0.0
dpGAN $\epsilon = 1$	874.663, 0.0	86.631, 0.0	1.135, 0.0	12.234, 0.0	4.794, 0.0	118.286, 0.0
dpGAN $\epsilon = 10$	1029.971, 0.0	88.122, 0.0	2.002, 0.0	9.876, 0.0	4.759, 0.0	93.632, 0.0
dpGAN $\epsilon = 100$	821.636, 0.0	89.354, 0.0	0.664, 0.0	9.982, 0.0	4.613, 0.0	82.561, 0.0
dpGAN $\epsilon = \infty$	1120.553, 0.0	81.773, 0.0	$1.359, 0.3e-5$	16.868, 0.0	6.248, 0.0	188.991, 0.0

## C.2. Population Statistics

In order to evaluate fidelity on a population scale, we compute a common set of glucose metrics used to evaluate patient glycemic control on the real and synthetic data, including average trace variability (VAR), Time in Range (TIR), the percentage of time glucose is within the clinical guided range of 70-180mg/dL; and time hypo- and hyper- glycemic (time below and above range, respectively) in Table 5. More details on each of the metrics are included in Table 4. We test if the difference in metrics between the synthetic and real data is statistically significant, using a p-value of 0.05. A p-value  $< 0.05$  indicates the difference is statistically significant. We want synthetic data that has similar population statistics to the real data: p-values  $> 0.05$  such that the differences in statistics between real and synthetic data are not significant. GlucoSynth outperforms all other models, with no statistically significant difference in all metrics for privacy budgets of  $\epsilon \geq 100$  and only one metric with a statistically significant difference for budgets  $\epsilon = 1 - 10$ .

## C.3. Distributional Comparisons

We visualize differences in distributions between the real and synthetic data by plotting the distribution of variances and using PCA (Bryant & Yarnold, 1995). Figure 6 and Figure 13 show the variance distribution and PCA plots, respectively for

the nonprivate models. We also compare distributional changes across privacy budgets: Figures 14 and 15 show GlucoSynth, Figures 16 and 17 show RGAN and Figures 18 and 19 show dpGAN.

Looking at the figures, GlucoSynth better captures the distribution of the real data compared to all of the nonprivate models. As evidenced in the PCA plot, (Fig. 13), FF comes the closest to capturing the real distribution in its synthetic data, but ours does a better job of representing the more rare types of traces. GlucoSynth also outperforms all of the private models across all privacy budgets. Even at small budgets ( $\epsilon < 1$ ), the general shape of the overall distribution is conserved (e.g., see Figure 14).

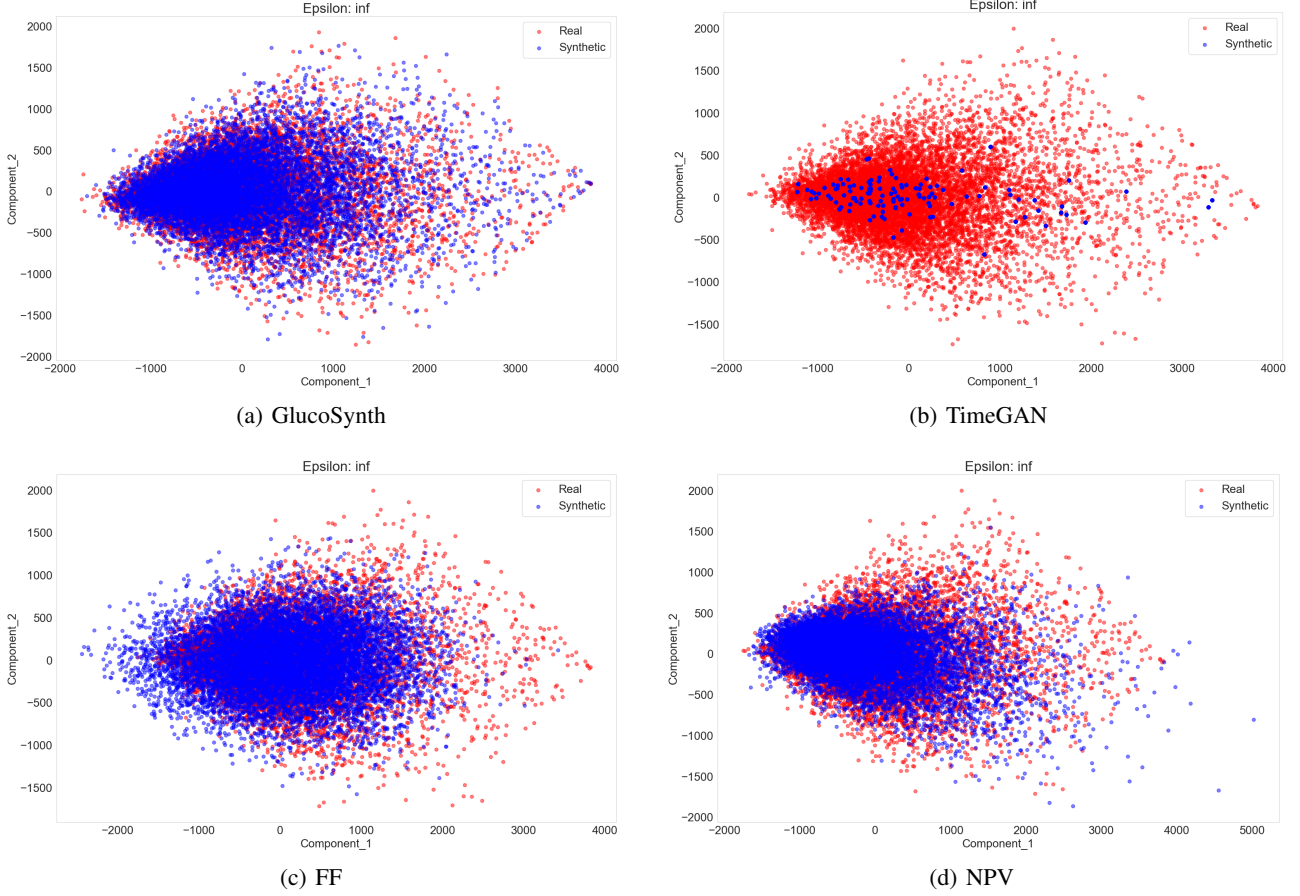


Figure 13. PCA Comparison for Nonprivate Models



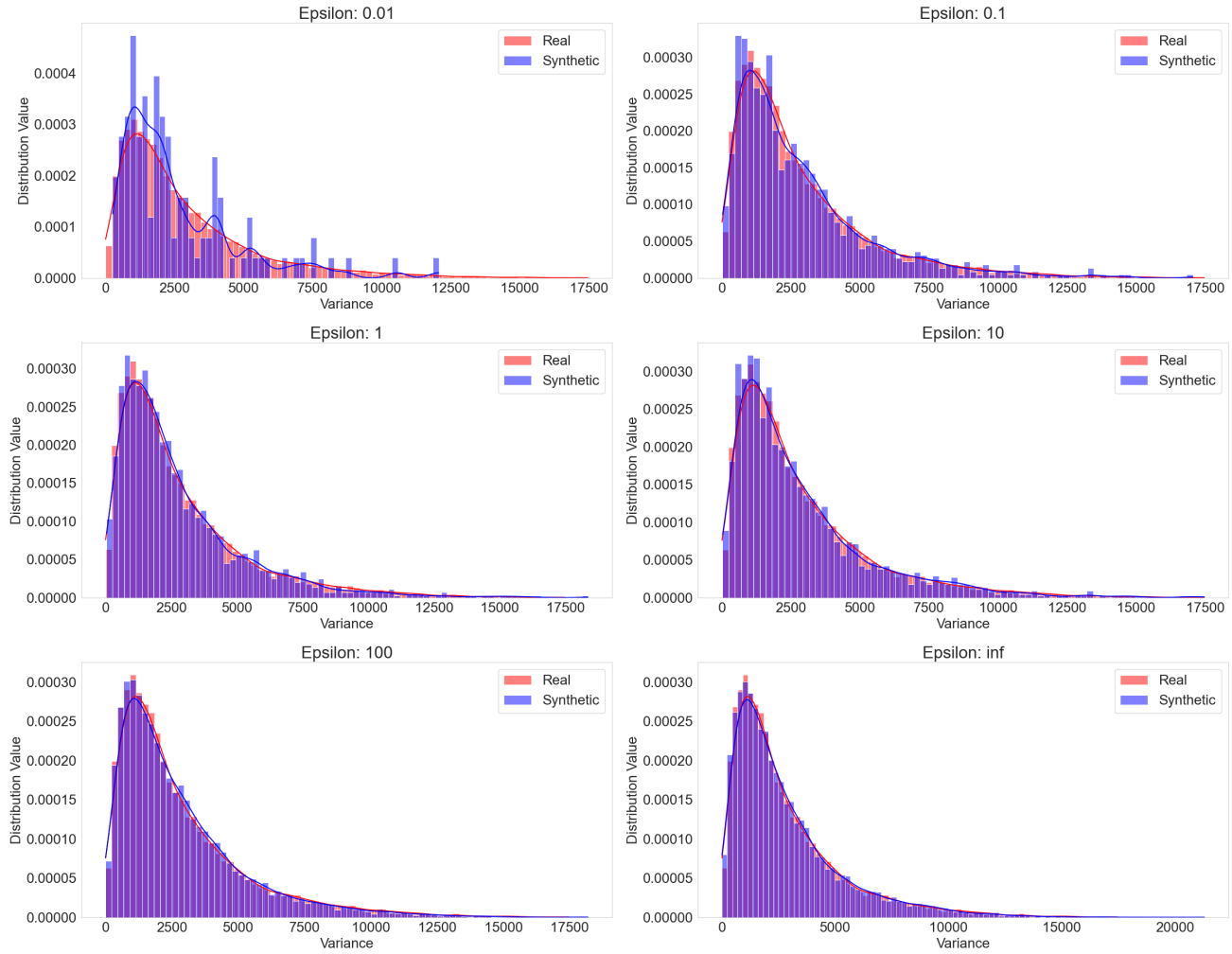


Figure 14. GlucoSynth distributional Variance Comparison Across Privacy Budgets

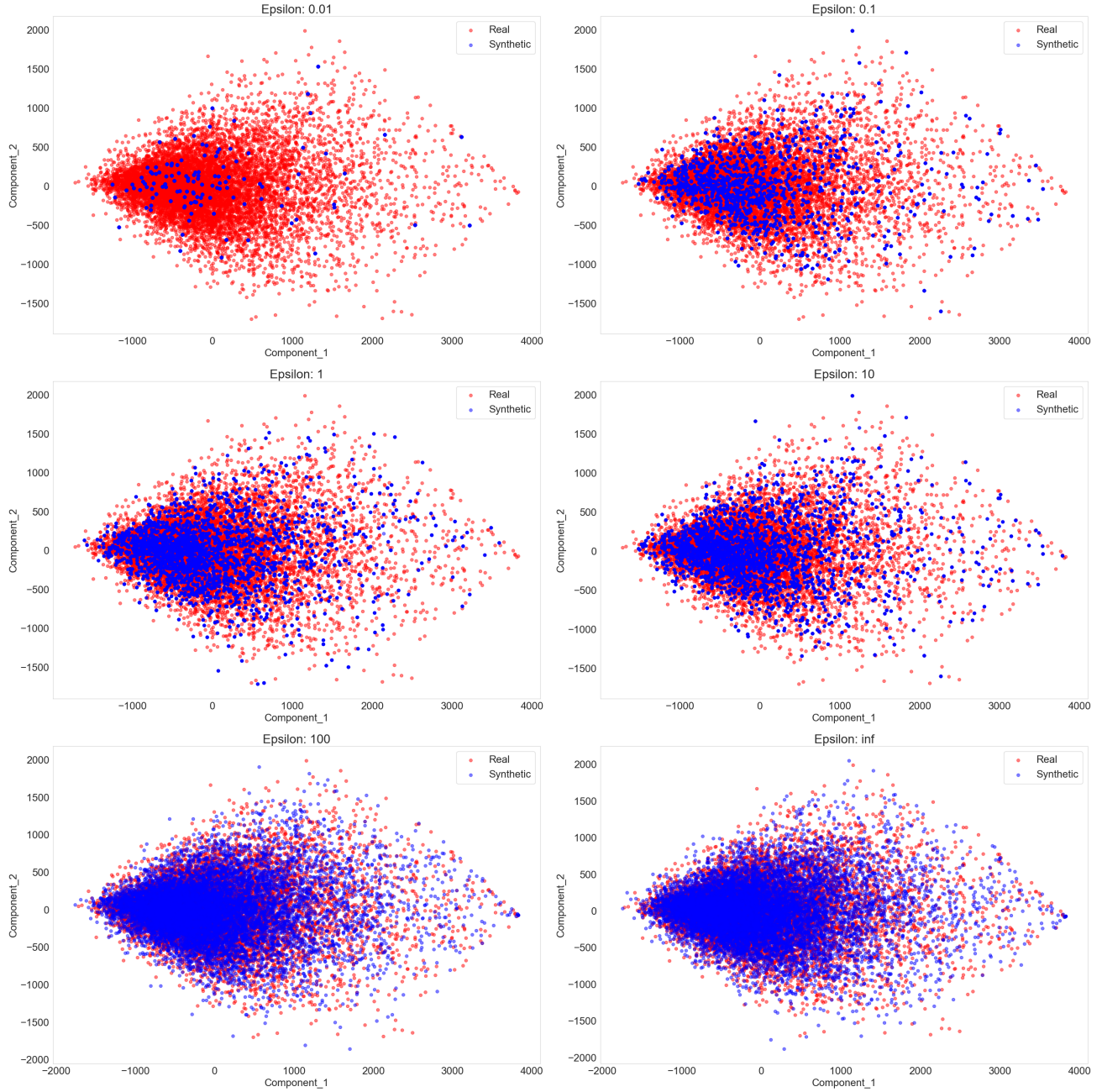


Figure 15. GlucoSynth PCA Comparison Across Privacy Budgets

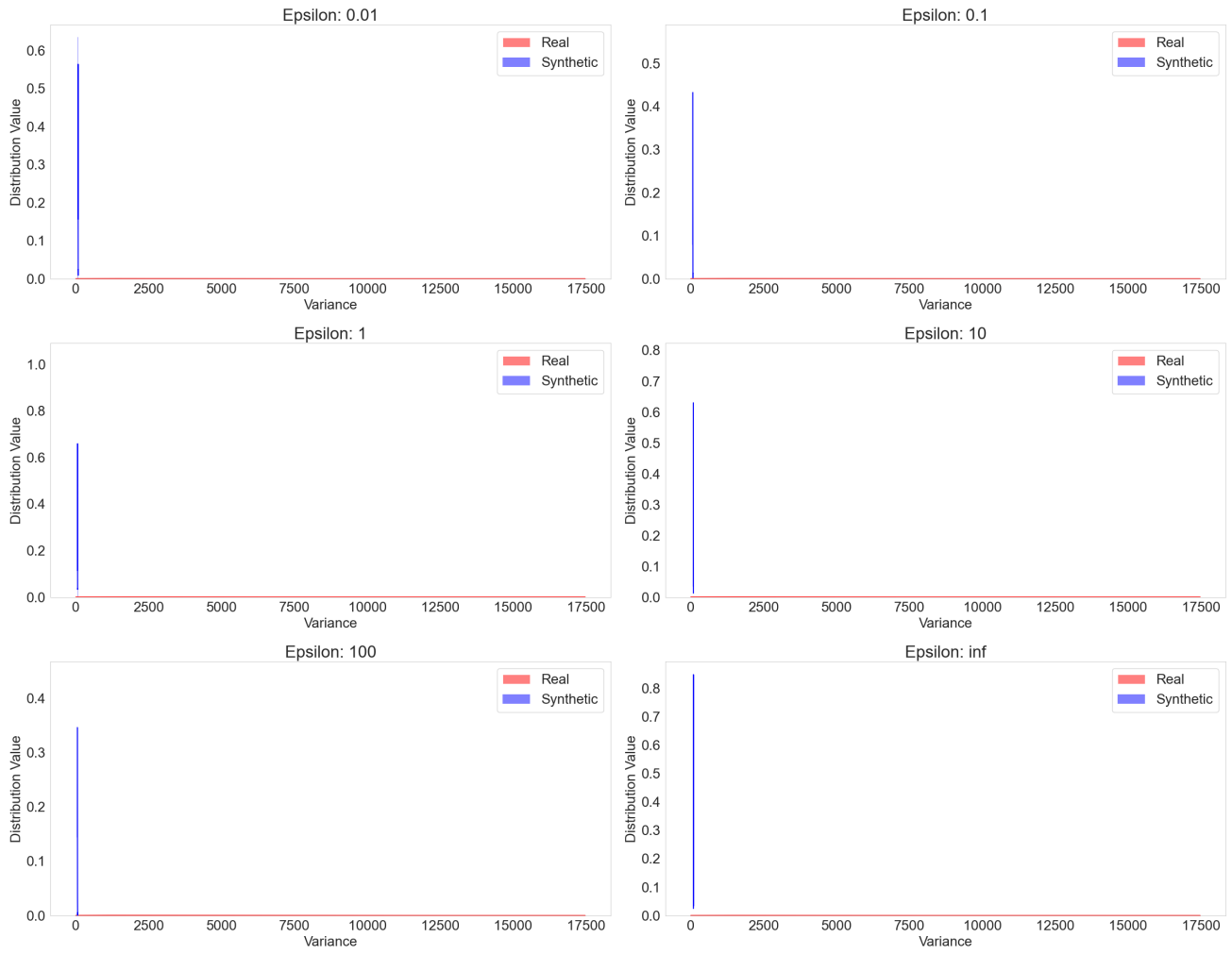


Figure 16. RGAN distributional Variance Comparison Across Privacy Budgets

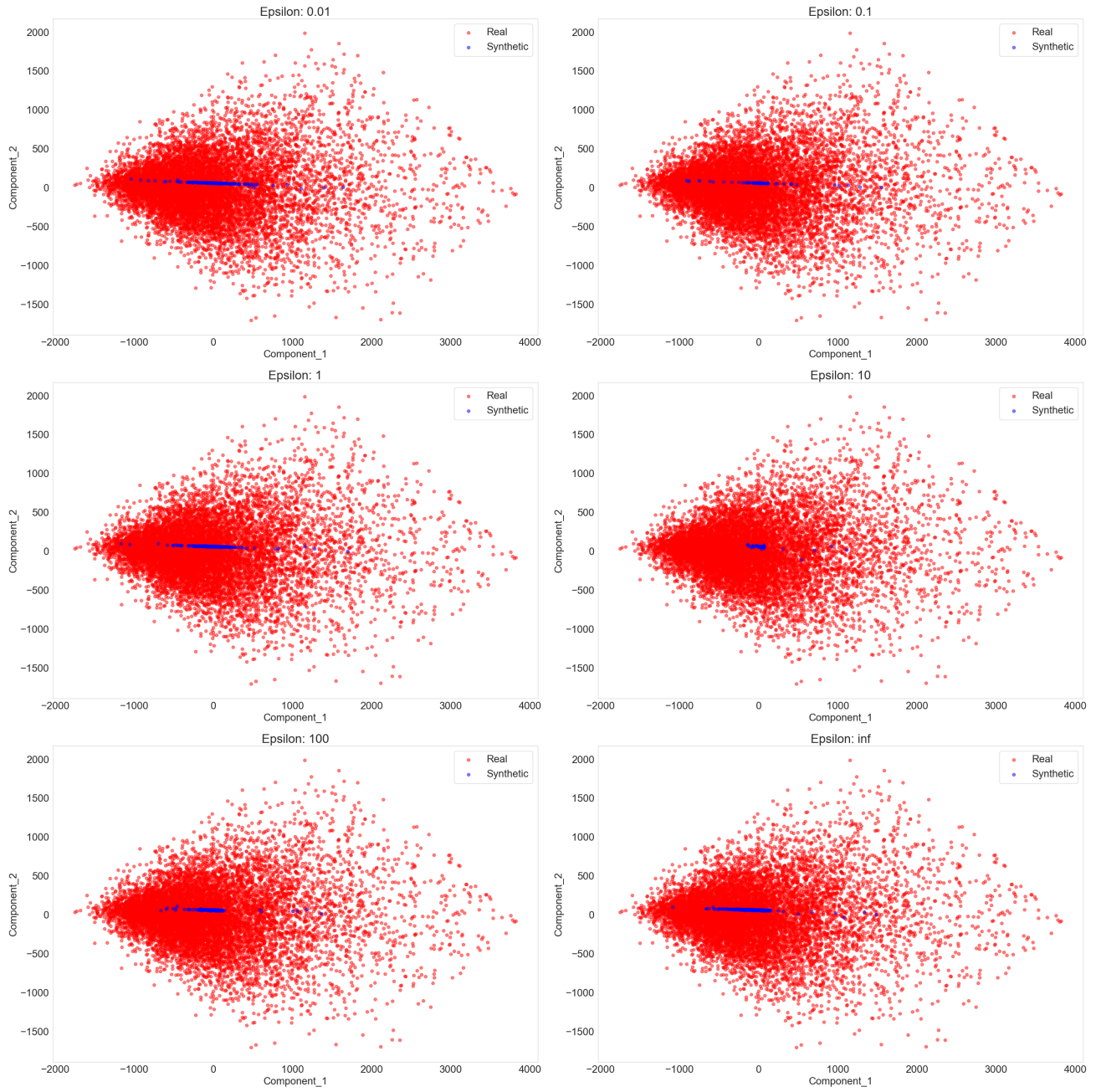


Figure 17. RGAN PCA Comparison Across Privacy Budgets



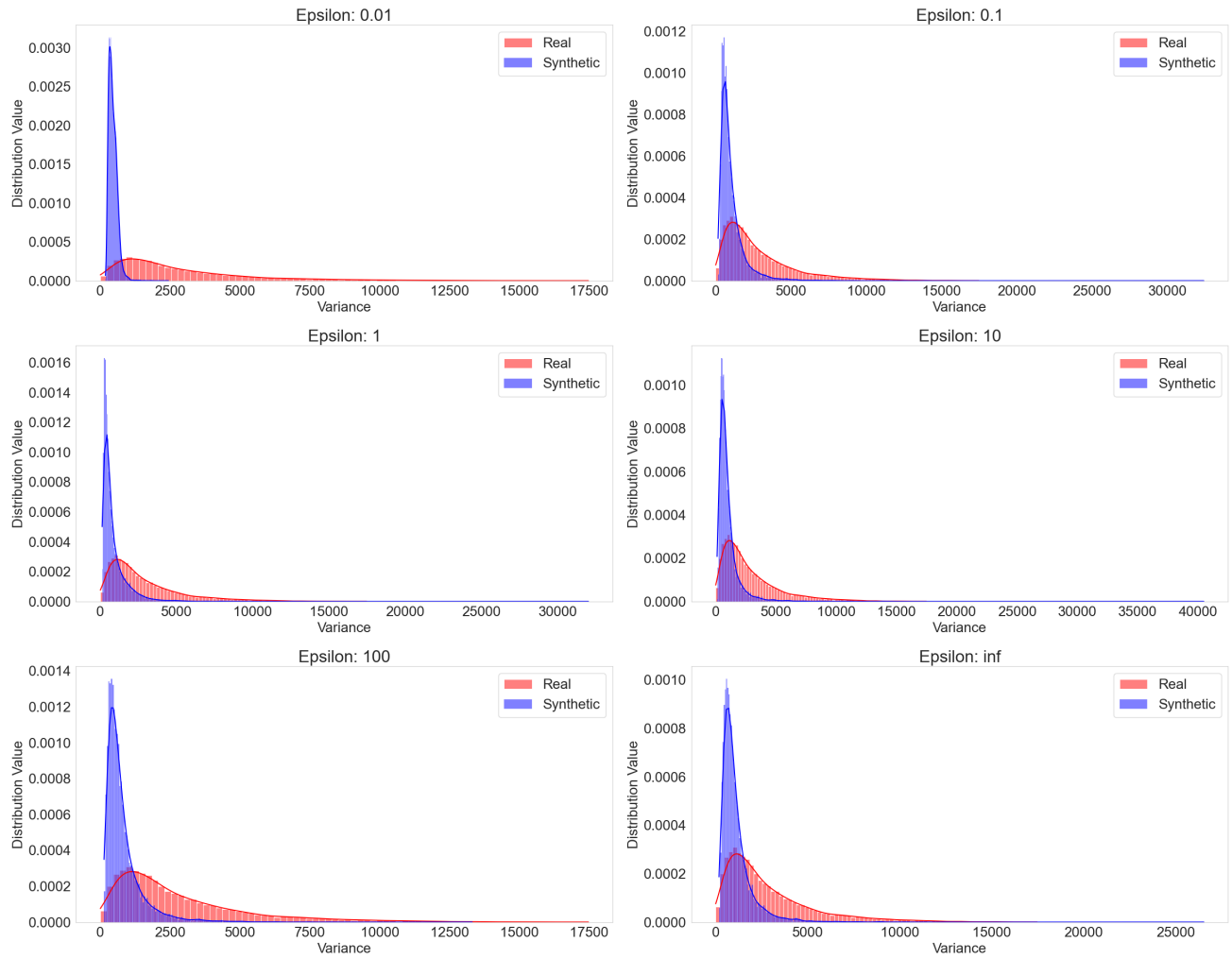


Figure 18. dpGAN distributional Variance Comparison Across Privacy Budgets

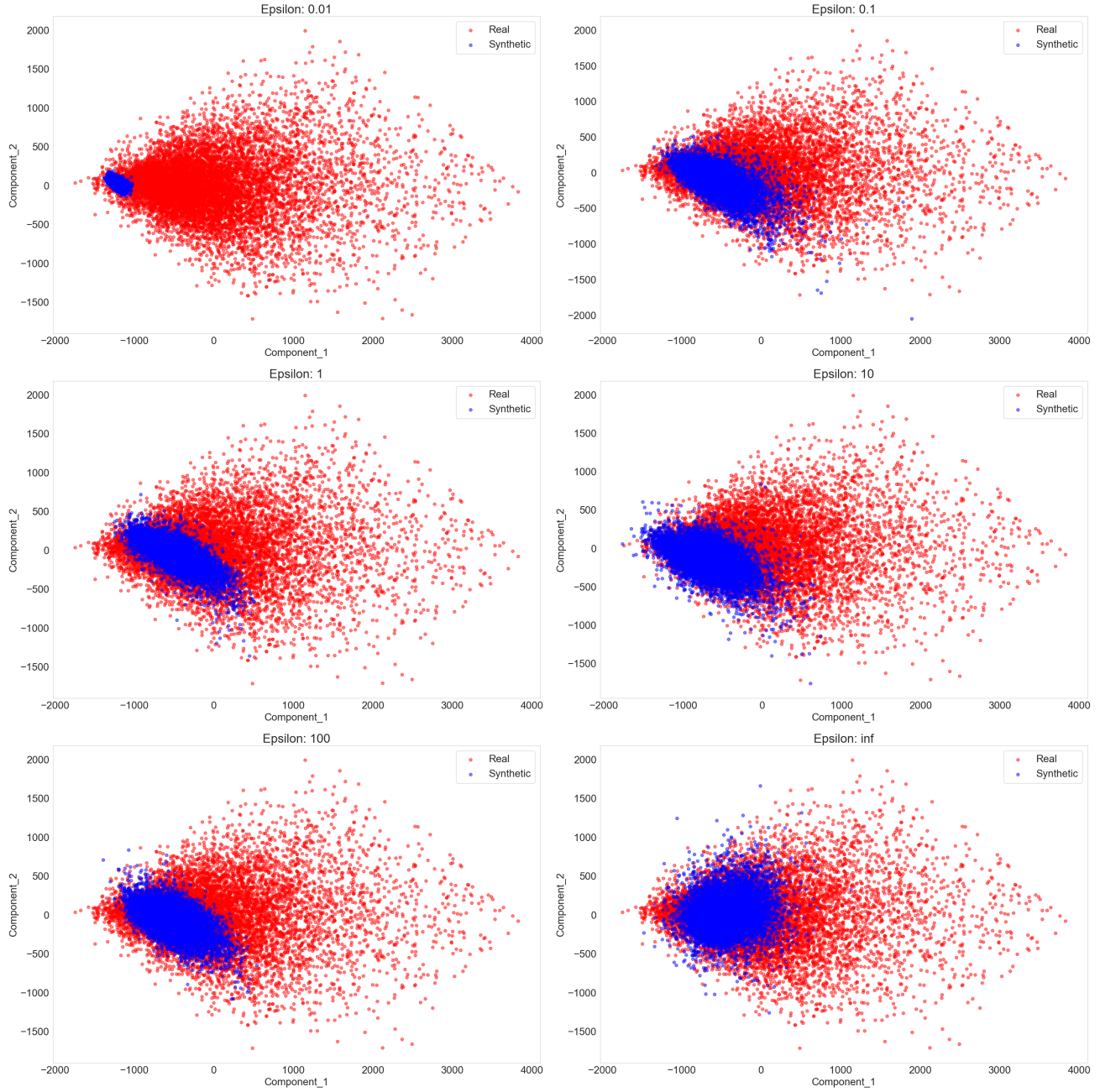


Figure 19. dpGAN PCA Comparison Across Privacy Budgets

## D. Additional Evaluation: Breadth

Compared to all other models across all privacy budgets, our model has the best ratio of true to fake motifs, with close to 1.0 for %TM, with correspondingly low %FM and the lowest MSEs. It also has the best coverage for nonprivate settings and an  $\epsilon$  of 100. Interestingly, dpGAN has the best coverage compared to all other models for privacy budgets  $\epsilon \leq 10$  but worse MSEs across all budgets than GlucoSynth. This means that although it finds a broader *number* of motifs contained in the real data, the overall distributions of motifs it creates in the synthetic data have much higher error rates. We argue that the tradeoff found by our model is better because although it does miss some of the *types* of motifs from the real data (misses some breadth), from the ones it does find it constructs realistic distributions of the motifs and generates very few fake ones.

## E. Additional Evaluation: Utility

Since RMSE may provide a limited view about the predictions from the glucose forecasting model, we also plot the Clarke Error Grid (Clarke, 2005), which visualizes the differences between a predictive measurement and a reference measurement, and is the basis used for evaluation of the safety of diabetes-related medical devices (for example, used for evaluating glucose outputs from predictive models integrated into artificial insulin delivery systems). The Clarke Error Grid is implemented using [www.github.com/suetAndTie/ClarkeErrorGrid](https://www.github.com/suetAndTie/ClarkeErrorGrid). The grids are shown in Figure 20.

In the figures, the x-axis is the reference value and the y-axis is the prediction. A diagonal line means the predicted value is exactly the same as the reference value (the best case). There are 5 total zones that make up the grid, listed in order from best to worst:

- Zone A – Clinically Accurate: Predictions differ from actual values by no more than 20% and lead to clinically correct treatment decisions.
- Zone B – Clinically Acceptable: Predictions differ from actual values by more than 20% but would not lead to any treatment decisions.
- Zone C – Overcorrections: Acceptable glucose levels would be corrected (overcorrection).
- Zone D – Failure to Detect: Predictions lie within the acceptable range but the actual values are outside the acceptable range, resulting in a failure to detect and treat errors in glucose.
- Zone E – Erroneous Treatment: Predictions are opposite the actual values, resulting in erroneous treatment, opposite of what is clinically recommended.

We show Clarke Error grids for all models (and the private models with no privacy included,  $\epsilon = \infty$ ). This is because comparing the models at different privacy budgets is not very informative – it can be hard to tell exactly where changes between different budgets may occur. We also present a table with the percentages of predicted datapoints in each category in Table 6. This table includes a comparison among different privacy budgets for the private models (much more effective than the figures by themselves.)

Looking at the grids, we can see that GlucoSynth performs the best, with most of the values along the diagonal axis (Zone A and B) and less around the other zones (Zones C-E) as compared to the other models. This means that most of the predicted glucose values from the model trained on our synthetic data are in the Clinically Accurate and Acceptable ranges, with less in the erroneous zones. Moreover, by examining the table we see that GlucoSynth outperforms all other models across all privacy budgets as well.

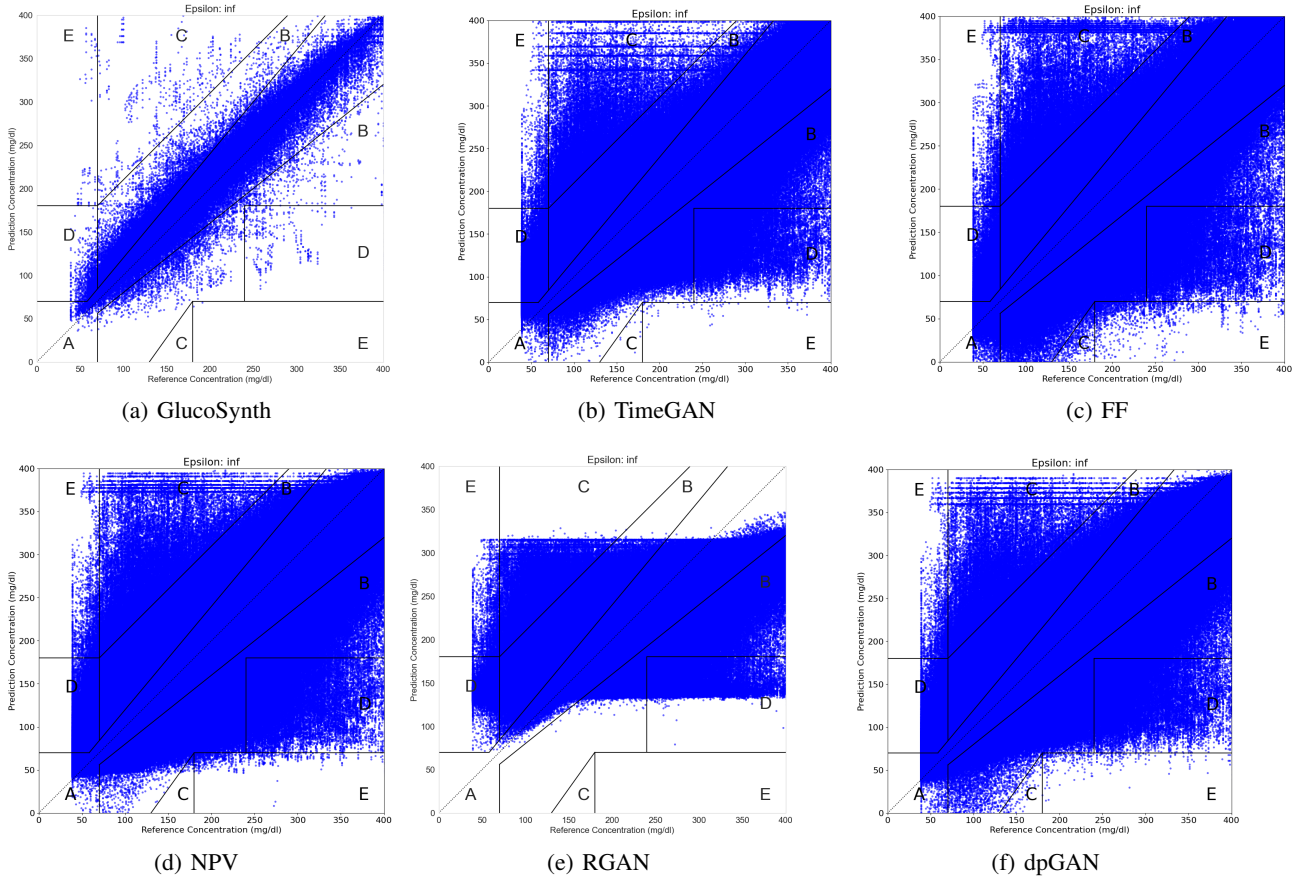


Figure 20. Clarke Error Zone Figures for All Models

 Table 6. Clarke Error Grid Zones. Value is the percentage of predicted datapoints. Categories go from A to E, best to worst. Bolded rows indicate the best results on the synthetic data at each privacy budget (nonprivate models compared with private models when  $\epsilon = \infty$ )

Model	A: Accurate	B: Acceptable	C: Overcorrection	D: Failure to Detect	E: Error
GlucoSynth $\epsilon = 0.01$	<b><math>0.858 \pm 1.057e-3</math></b>	<b><math>0.131 \pm 1.172e-3</math></b>	<b><math>3.271e-3 \pm 0.0</math></b>	<b><math>0.017 \pm 1.158e-4</math></b>	<b><math>5.79e-6 \pm 1.2e-6</math></b>
GlucoSynth $\epsilon = 0.1$	<b><math>0.863 \pm 6.947e-3</math></b>	<b><math>0.126 \pm 7.526e-4</math></b>	<b><math>3.054e-3 \pm 1.45e-5</math></b>	<b><math>0.018 \pm 4.34e-5</math></b>	<b><math>5.79e-6 \pm 0.0</math></b>
GlucoSynth $\epsilon = 1$	<b><math>0.862 \pm 1.578e-3</math></b>	<b><math>0.128 \pm 1.259e-3</math></b>	<b><math>3.343e-3 \pm 1.45e-5</math></b>	<b><math>0.016 \pm 3.329e-4</math></b>	<b><math>5.79e-6 \pm 0.0</math></b>
GlucoSynth $\epsilon = 10$	<b><math>0.864 \pm 6.947e-3</math></b>	<b><math>0.125 \pm 6.513e-4</math></b>	<b><math>3.039e-3 \pm 5.79e-5</math></b>	<b><math>0.017 \pm 4.34e-5</math></b>	<b><math>8.68e-6 \pm 2.89e-5</math></b>
GlucoSynth $\epsilon = 100$	<b><math>0.864 \pm 1.74e-3</math></b>	<b><math>0.126 \pm 1.447e-3</math></b>	<b><math>3.387e-3 \pm 0.0</math></b>	<b><math>0.017 \pm 2.895e-4</math></b>	<b><math>5.79e-6 \pm 0.0</math></b>
GlucoSynth $\epsilon = \infty$	<b><math>0.964 \pm 1.201e-3</math></b>	<b><math>0.035 \pm 1.158e-3</math></b>	<b><math>3.039e-4 \pm 2.89e-5</math></b>	<b><math>1.732e-4 \pm 1.158e-4</math></b>	<b><math>8.68e-6 \pm 1.45e-5</math></b>
TimeGAN	$0.741 \pm 0.012$	$0.233 \pm 0.012$	$2.240e-3 \pm 9.8e-5$	$0.024 \pm 8.44e-4$	$2.19e-4 \pm 1.9e-5$
FF	$0.824 \pm 6.624e-3$	$0.156 \pm 6.148e-3$	$3.547e-3 \pm 9.0e-5$	$0.017 \pm 3.940e-4$	$3.57e-4 \pm 8.0e-6$
NPV	$0.79 \pm 3.03e-4$	$0.186 \pm 3.87e-4$	$3.49e-3 \pm 1.5e-5$	$0.02 \pm 1.04e-4$	$3.58e-4 \pm 5.0e-6$
RGAN $\epsilon = 0.01$	$0.54 \pm 0.014$	$0.435 \pm 0.014$	$3.389e-4 \pm 1.197e-4$	$0.024 \pm 2.71e-4$	$2.429e-4 \pm 3.43e-5$
RGAN $\epsilon = 0.1$	$0.594 \pm 1.998e-3$	$0.38 \pm 1.74e-3$	$1.326e-3 \pm 1.429e-4$	$0.025 \pm 1.069e-4$	$2.873e-4 \pm 8.68e-6$
RGAN $\epsilon = 1$	$0.637 \pm 6.785e-3$	$0.336 \pm 6.128e-3$	$2.661e-3 \pm 1.87e-5$	$0.024 \pm 6.464e-4$	$2.792e-4 \pm 2.95e-5$
RGAN $\epsilon = 10$	$0.634 \pm 3.452e-3$	$0.338 \pm 3.247e-3$	$2.253e-3 \pm 1.004e-4$	$0.025 \pm 2.894e-4$	$3.027e-4 \pm 1.71e-5$
RGAN $\epsilon = 100$	$0.638 \pm 4.709e-3$	$0.335 \pm 4.219e-3$	$1.991e-3 \pm 2.17e-5$	$0.025 \pm 4.884e-4$	$2.949e-4 \pm 2.26e-5$
RGAN $\epsilon = \infty$	$0.646 \pm 6.89e-4$	$0.326 \pm 7.19e-4$	$2.613e-3 \pm 2.852e-4$	$0.024 \pm 3.006e-4$	$2.859e-4 \pm 1.5e-5$
dpGAN $\epsilon = 0.01$	$0.308 \pm 3.482e-3$	$0.509 \pm 3.71e-3$	$2.894e-7 \pm 0.0$	$0.183 \pm 2.33e-4$	$1.114e-5 \pm 4.196e-6$
dpGAN $\epsilon = 0.1$	$0.781 \pm 6.35e-4$	$0.191 \pm 5.37e-4$	$3.226e-3 \pm 5.715e-5$	$0.024 \pm 3.8e-5$	$2.533e-4 \pm 1.881e-6$
dpGAN $\epsilon = 1$	$0.786 \pm 5.44e-4$	$0.187 \pm 5.81e-4$	$2.409e-3 \pm 2.894e-7$	$0.024 \pm 3.6e-5$	$2.078e-4 \pm 5.787e-7$
dpGAN $\epsilon = 10$	$0.806 \pm 7.34e-4$	$0.169 \pm 6.09e-4$	$2.386e-3 \pm 1.476e-5$	$0.023 \pm 1.113e-4$	$2.146e-4 \pm 2.749e-6$
dpGAN $\epsilon = 100$	$0.813 \pm 3.18e-4$	$0.161 \pm 2.86e-4$	$2.266e-3 \pm 2.083e-5$	$0.023 \pm 5.4e-5$	$1.889e-4 \pm 1.013e-6$
dpGAN $\epsilon = \infty$	$0.819 \pm 1.487e-3$	$0.16 \pm 1.306e-3$	$3.193e-3 \pm 2.677e-5$	$0.018 \pm 1.60e-4$	$3.166e-4 \pm 5.208e-6$